SEMARAK ILMU PUBLISHING

Journal of Advanced Research in Fluid Mechanics and Thermal Sciences

Journal homepage:
https://semarakilmu.com.my/journals/index.php/fluid_mechanics_thermal_sciences/index
ISSN: 2289-7879

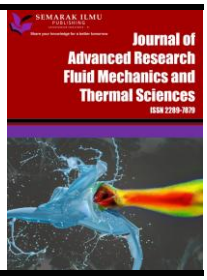

Base Pressure Control using Quarter Rib at Mach 1.3: A Comprehensive CFD Analysis

Shamitha Shetty[1], Fharukh Ahmed Ghasi Mahaboobali[2], Ambareen Khan[3], Mohmmad Nishat Akhtar[4], Sher Afghan Khan[5,*], Khizar Ahmed Pathan[6]

[1] Department of Mathematics, Nitte Meenakshi Institute of Technology Bangalore, Affiliated to VTU, 560064, India
[2] Government Engineering, College Gangavathi Koppal, District Karnataka, India
[3] Centre for Instructional Technology and Multimedia, Universiti Sains Malaysia, Pinang, Malaysia
[4] School of Aerospace Engineering, Universiti Sains Malaysia, 14300 Nibong Tebal, Penang, 11600, Malaysia
[5] Department of Mechanical & Aerospace Engineering, Faculty of Engineering, IIUM, Gombak Campus, Kuala Lumpur, Malaysia
[6] Department of Mechanical Engineering, CSMSS Chh. Shahu College of Engineering, Aurangabad, Maharashtra, India

ARTICLE INFO

Article history:
Received 2 October 2024
Received in revised form 6 January 2025
Accepted 17 January 2025
Available online 20 February 2025

Keywords:
Base pressure; L/D ratio; Mach number; sudden expansion; nozzle pressure ratio

ABSTRACT

The study of base pressure and its control is an important research area in the transonic speed when the flow undergoes a sudden change in area. The turbulent flow in a separated region is still a crucial area of research due to the advent of space shuttles and high-performance military aircraft, and turbulent flow in transonic and supersonic flow is a thrust area for researchers. This paper focuses on base pressure control with sudden expansion at Mach 1.3 for an area ratio of 4.84. The flow field inside the duct is controlled through a passive control in the form of quarter ribs of radii 1 mm, 2 mm, 3 mm, and 4 mm for various duct lengths in the range from L = 1D to 6D for nozzle pressure ratios in the range from 3 to 11. Results show that a 1 mm rib is not adequate, and rib radii 2 mm, 3 mm, and 4 mm are effective in raising the base pressure values, and this rise in the base pressure continues till the duct length L = 1D to 4D. There is a marginal reduction in base pressure for the duct lengths L = 5D and 6D due to the ineffectiveness of the back pressure.

1. Introduction

Sudden expansion of the duct area is a widely studied phenomenon in various flow systems. Due to the sudden increase in the region, the flow sees a large area to expand and will undergo expansions. The shear layer exiting from the nozzle will undergo expansion, and the flow separation and reattachment with the duct wall characterize the flow. The enlarged duct is often smooth and continuous within, using the low base pressure that results from the sudden relaxation of the shear layer from the intake channel at the entry to the sudden enlargement. The flow field downstream of the base will be separated and sub-atmospheric. The vortex dynamics of the sudden flow expansion in the more extensive duct determines the base pressure. The total drag coefficient consists of skin-

* *Corresponding author.*
E-mail address: sakhan@iium.edu.my

https://doi.org/10.37934/arfmts.127.2.132

friction drag co-efficient, wave drag co-efficient, and base drag co-efficient. Out of these three on skin friction drag, we do not have any control as it is demand-driven and based on the user's requirement. As far as wave drag is concerned, from the literature, it is found that if the nose finess ratio is 2.5 to 4, the wave drag will be at its lowest value.

Hence, finally, we are left with the base drag, which can be controlled to reduce the aerospace vehicles' net drag. The literature also found that the base drag contribution can be as high as 60 to 70 percent of the total drag of the body of the revolution. As the contribution of the base drag is significant, any increase in the base pressure value will result in a considerable decrease in the total drag. Consequently, it will increase the range of missiles, unguided rockets, bombs, shells, etc., leading to significant savings in fossil fuels and reduced air pollution and, ultimately, global warming.

Nevertheless, before the jet is exhausted into the environment, our work focuses on air jets that suddenly develop into a larger duct with annular ribs. In the present study, the base pressure and the growth of the flow field downstream of the base zone are produced by the combined action of the primary vortices, which are formed by the free expansion of the shear layer at the base, and the secondary vortices, which are created by the ribs in the more substantial duct. A couple of the works that directly affect the current study are discussed.

However, the emphasis is on air jets that empty into the environment after suddenly expanding into a more extensive duct, including annular ribs. Together, the primary vortices from the free expansion of the shear layer at the base and the secondary vortices from the cavities in the enlarged duct provide the base pressure and the growth of the flow field downstream of the base zone in the current work. As far as the authors know, no one has ever tried the quarter rib circle as the control mechanism for base pressure. So far, researchers have used rectangular, semi-circular, triangular ribs. Among all these three ribs, the rectangular Rib was most effective in regulating the base pressure as two secondary vortices were created at the two sharp corners of the ribs; later, it was found that the triangular Rib was also, but the increase in the base pressure was less as compared to the rectangular ribs. Among them, the semi-circular Rib was the least effective as the flow sees a smooth variation in the control shape and does not generate any powerful secondary vortices. This study will fill the research gap as we use passive control in the form of quarter circular ribs at low supersonic Mach numbers. At this Mach number M = 1.3, the base pressure is lower than the ambient pressure, and the contribution from the base drag due to this low base pressure can be around seventy percent of the total drag, which is significant. Therefore, even a slight increase in the base pressure will decrease the aerospace vehicles' base drag and overall drag.

2. Literature Review

In this section, we will scan the literature on the base pressure control in a suddenly expanded flow. There are two methods of control: (i) Passive control and (ii) Active control. Passive control can be accomplished by altering the geometry whenever the active control mechanism is used. It requires an external source of energy, which is very complex if the same is not available through the propulsion system of the aerospace system. Pathan *et al.*, [1,2] elucidated that optimizing expansion geometry can markedly enhance base flow characteristics, thereby underscoring the pivotal role of design in augmenting aerodynamic performance. In a complementary study, Fiqri *et al.*, [3] explored control mechanisms within suddenly expanded flows characterized by cavities at sonic Mach numbers, revealing that a strategically designed cavity serves as an effective passive control strategy; this innovation not only improves flow reattachment but also elevates base pressure. Similarly, Asadullah *et al.*, [4] advocated for a cost-effective, passive technique to reduce base drag, broadening the accessibility of aerodynamic optimization. Moreover, Pathan *et al.*, [5] further studied how

optimizing the duct lengths enhances flow management and minimizes pressure losses in expanded flows, reinforcing the geometric design's significance. However, these findings collectively suggest that design considerations are not merely superficial but fundamentally integral to aerodynamic efficiency.

Pathan *et al.*, [6] investigated the impact of varying expansion levels on base pressure and the associated reattachment length; they discovered that an optimized expansion geometry significantly enhances base flow characteristics. Similarly, Azami *et al.*, [7] investigated the dynamics of supersonic flows within converging-diverging nozzles, explaining how different nozzle configurations can modify flow patterns, thereby advancing passive control strategies in supersonic contexts. Furthermore, Pathan *et al.*, [8] demonstrated that the optimization of nozzle design, mainly through the manipulation of variable wall thickness, not only enhances performance but also contributes to a reduction in structural weight; this showcases the manifold advantages of innovative geometric methodologies in the realm of aerospace engineering.

The research underscores the potential inherent in passive and active control methodologies for optimizing flow characteristics in high-speed aerodynamic configurations [9-11]. Passive design modifications, such as meticulously devised geometries, have demonstrated efficacy in enhancing efficiency without necessitating active control mechanisms [12-19]. However, integrating sophisticated computational tools, including Computational Fluid Dynamics (CFD), into traditional frameworks presents challenges, primarily due to the intricate nature of fluid dynamics [20,21].

Computational Fluid Dynamics (CFD) has garnered significant attention across many domains. Chaudhari *et al.*, [22] elucidated that the combustion strategies employed in series catalytic converters exert a considerable influence on fluid dynamics, thereby providing valuable insights into sonic aerodynamic flows. Jain *et al.*, [23] illustrated that the orientation of heat sinks has a profound effect on thermal performance; this underscores the essential nature of geometric optimization in heat transfer and flow management. Furthermore, Khalil *et al.*, [24] delved into the complexities of air jet heat transfer, revealing the interplay between airflow dynamics and thermal or aerodynamic design principles. Moreover, previous studies harnessed the power of CFD to enhance flow uniformity in catalytic converters, emphasizing its critical importance in increasing base pressure and flow characteristics and advancing aerodynamic applications [25-28].

An extensive review has investigated the intricate dynamics of base pressure control in high-speed flows, employing passive control methodologies such as ribs and nozzle optimization. Khan *et al.*, [29-31] have convincingly demonstrated that incorporating quarter and semi-circular ribs within suddenly expanded ducts leads to a notable enhancement in flow reattachment, significantly mitigating base drag. Similarly, Nurhanis *et al.*, [32] and Khan *et al.*, [33,34] have underscored the pivotal role of nozzle geometry in stabilizing fluid dynamics and optimizing base pressure across sonic and supersonic Mach numbers. Furthermore, numerical studies conducted by Khan *et al.*, [35-37] have further emphasized the critical influence of area ratios in managing flow separation.

Rathakrishnan [38] studied the effect of Rib in a suddenly expanded flow at sonic Mach numbers. He conducted experiments at various nozzle pressure ratios ranging from 1.141 to 2.54 for 3:1, 3:2, and 3:3 rib aspect ratios. His investigation revealed a decreasing trend in the base pressure at a lower aspect ratio, and control decreases the base pressure. The base pressure increased when an aspect ratio of 3:3 Rib was employed. Therefore, depending upon the end user's demands, these combinations of the ribs can be used. If the mission requirement is to increase the base pressure, then the Rib with an aspect ratio is ideal. The Rib with an aspect ratio of 3:1 is the right choice when the application is in a combustion chamber. In the present study, we have validated our CFD results first with the experimental results of Rathakrishnan [38]. After validation, we took various rib geometry, rib location, and nozzle pressure ratios to study passive control's effect on base pressure.

However, these studies show the necessity of continued research in this area, as the interdependencies among various factors remain fully understood. Although promising, this endeavor requires further investigation because the complexities involved are substantial. From the above review, it is evident that there is research on low supersonic Mach numbers, and more so so far, none of the researchers has ever used quarter rib circles.

3. Computational Fluid Dynamics Analysis

3.1 Governing Equations

The following hypotheses are taken into consideration:

i. Turbulent flow is considered because of the turbulent viscous dissipation effects.
ii. The fluid's viscosity varies with temperature and is compressible.
iii. At atmospheric pressure, the flow exits the duct.
iv. While scanning the literature, we found that the internal flow k-epsilon turbulence model is the best as it gives reasonably good results. Shaikh *et al.*, [16] employed the usual k-epsilon turbulence model to simulate internal flow. As a result, the standard k-epsilon turbulence model is applied to the circumstance. Sutherland's three-coefficient viscosity model is expressed as follows:

$$\mu' = \mu'_o \left(\frac{T_a}{T_{a,o}}\right)^{3/2} \frac{T_{a,o}+S\prime}{T_a+S\prime} \tag{1}$$

The reference viscosity value in kg/m-s is denoted as μ'o,, where μ' represents the viscosity. Ta denotes static temperature, K represents the temperature of a standard reference, and S' is the temperature-dependent Sutherland constant. Three-dimensional continuity equation for compressible flow:

The equation for mass balance is as follows:

$$\frac{\partial \rho}{\partial t} + \underline{\nabla} \cdot \left(\rho \underline{V}\right) = 0 \tag{2}$$

where the fluid's velocity is denoted by V.

The equation for momentum balance is:

$$\frac{\partial}{\partial t}\left(\rho \underline{V}\right) + \underline{\nabla} \cdot \left(\rho \underline{V}\underline{V}\right) + \underline{\nabla} p = \underline{\nabla} \cdot \left[2\mu\left(\underline{\nabla V}\right)_o^s\right] + \underline{\nabla} \cdot \left(\tau_{=Re}\right) \tag{3}$$

Where $\left(\underline{\nabla V}\right)_o^s = \left(\underline{\nabla V}\right)^s - \frac{1}{3}\left(\underline{\nabla} \cdot \underline{V}\right)\underline{I}$, $\left(\underline{\nabla V}\right)^s = \frac{\underline{\nabla V} + \underline{\nabla V}^T}{2}$, and $\tau_{=Re}$ is the turbulent stress tensor.

The formulae for total energy are as follows:

$$\frac{\partial}{\partial t}\left[\rho\left(\frac{1}{2}V^2 + u_{int}\right)\right] + \underline{\nabla}\left[\rho\left(\frac{1}{2}V^2 + u_{int}\right)\underline{V}\right] = \underline{\nabla}\left(\lambda \underline{\nabla} T - p\underline{V} + 2\mu \underline{V} \cdot \left(\underline{\nabla V}\right)_o^s + \underline{V} \cdot \tau_{=Re}\right) \tag{4}$$

where u_{int} is the internal energy, and λ is the thermal conductivity.

Many internal flow simulations use the k-epsilon turbulence model due to its affordability, resilience, and sufficient accuracy. The Ansys Fluent program incorporates the k-epsilon (ε) turbulence model used in this research. The K-equation allowed us to calculate the turbulent kinetic energy.

$$\frac{\partial}{\partial t}(\rho k) + \underline{\nabla} \cdot \left(\rho \underline{V} k\right) = \underline{\nabla} \cdot \left[(\mu + \frac{\mu_t}{\sigma_k})(\underline{\nabla} k)\right] - \rho\varepsilon + M_x \tag{5}$$

The turbulent kinetic energy dissipation rate is denoted by ε, the turbulent Prandtl number is σ-k, and the word Mx is the turbulence generation. Precisely, the dissipation (or (-equation)) is controlled by,

$$\frac{\partial(\rho\varepsilon)}{\partial t} = -\underline{\nabla} \cdot \left(\rho\varepsilon\vec{V}\right) + \underline{\nabla} \cdot \left[\left(\mu + \frac{\mu_T}{\sigma_\varepsilon}\right)\nabla\varepsilon\right] - C_1 f_1 \left(\frac{\varepsilon}{k}\right) M - C_2 f_2 \frac{\varepsilon^2}{k} \tag{6}$$

where $\mu_t = \rho f_\mu C_\mu k^2/\varepsilon$ denotes turbulent viscosity, and the arbitrary constants are denoted as $\overline{C_\mu} = 0.09$, $\overline{C_1} = 1.44$, $\overline{C_2} = 1.92$, $\overline{f_\mu} = 1$, $\sigma_k = 1.0$, and $\sigma_\varepsilon = 1.3$.

3.2 Geometry and Modelling

The finite volume technique (FVM) was employed to delve further into this investigation. The CFD simulation used the ANSYS FLUENT 2024/R2 software to assess the nozzle's fluid flows. We are examining the impact of the quarter geometry of the Rib in the form of a passive control method. The orientation of the quarter rib is shown in Figure 1.

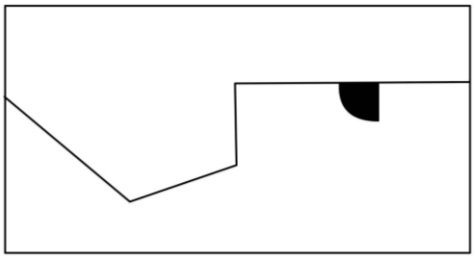

Fig. 1. Orientation of the Rib

3.3 Meshing and Boundary Conditions

A crucial part of the CFD process is meshing. By choosing the free-face mesh type, the 2D model is of the structured mesh type in this case. Elements were given sizes according to each line (edge) length when the constructed structured mesh type was used. The lines were utilized to apply the element size, and elements with identical forms were created using face meshing. The mesh independence check is done. Figure 2 below shows the mesh's element type and size tested during mesh independence check.

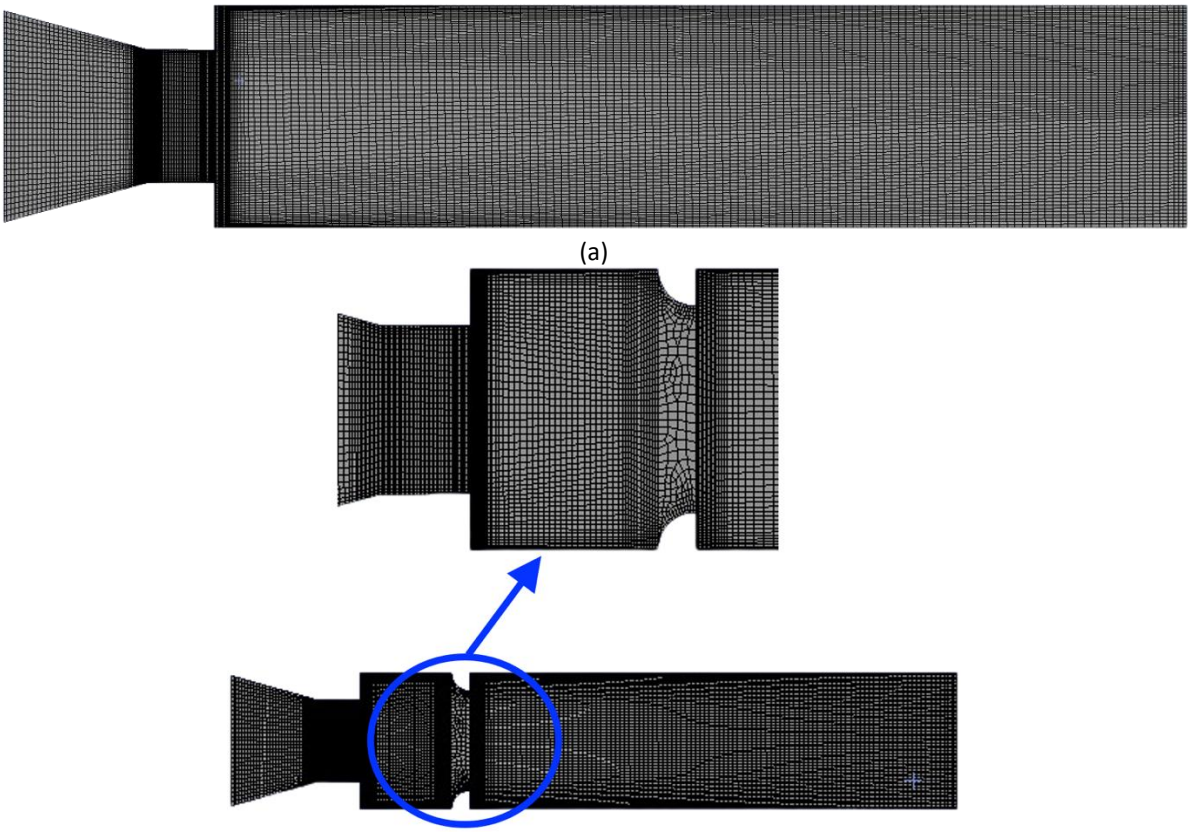

(a)

(b)

Fig. 2. Mesh Model (a) without ribs (b) with ribs

3.4 Assumptions and Fluid Properties

Assumptions are made to replicate the flow activities in the precise physical environment. Appropriate mathematical and numerical models are selected to simplify the governing equations.

To solve the governing equations simultaneously, numerical modeling requires choosing the appropriate mathematical models, such as the governing equations, boundary conditions, mesh quality, and numerical method. Despite its limitations in accurately representing physical phenomena, the computational method has been trusted for decades and offers sufficient insight into flow behavior. As a result, this calls for careful consideration of elements that closely resemble the flow behavior. This study pinpoints the presumptions that jeopardize the precise physical state. The following are the presumptions and characteristics covered in this study:

i. The flow is assumed to be a steady 2D flow because geometry is symmetric. Hence, the assumption that the flow is 2-D is justified.
ii. The density of the air is variable as the flow is compressible. The inlet pressure is the gauge pressure at that Mach number and NPR, and at the outlet of the duct, the gauge pressure at the outlet is zero.
iii. Since turbulent flow has a significant impact on turbulent viscous dissipation at a given flow velocity, it is taken into consideration.
iv. The viscosity of the fluid is dependent on temperature.
v. At the standard atmospheric pressure, the flows leave the duct. At normal ambient pressure, the flows leave the duct.

vi. Since the flow via the nozzle is considered turbulent, the compressible flow field is represented by the k-epsilon standard model. The subsequent equations most appropriately characterize the turbulent flow.

3.5 Geometry of the Model

The ANSYS Workbench program utilized fluid flow (Fluent) analytical techniques and was employed for the entire computational fluid dynamics (CFD) procedure. The model was generated via a Design Modeller. Figure 3 depicts a converging nozzle that abruptly widens into a duct with five ribs. In Rathakrishnan's [38] experimental setup, the dimensions of the convergent-divergent nozzle with a suddenly expanded duct are as stated in Table 1.

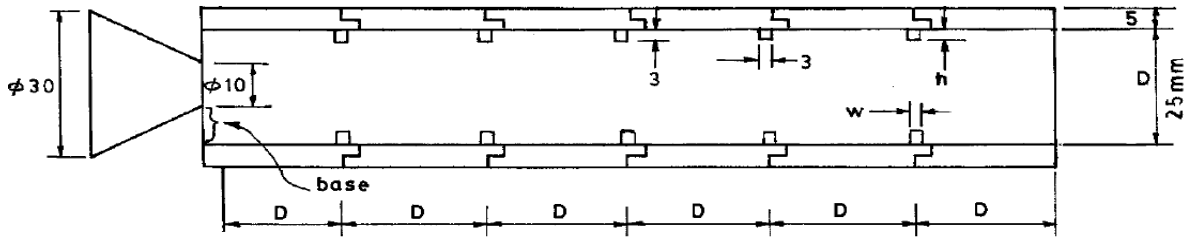

Fig. 3. Duct with five ribs used in an experimental study [38]

Table 1
The geometries of the validation model

Parameters	Dimensions
Nozzle inlet diameter	30 mm
Nozzle outlet diameter	10 mm
Duct diameter	25 mm
Duct length	Varies from 1D to 6D
Converging length	20 mm
Rib width	3 mm
Rib height	Varies from 1mm to 3mm

3.5.1 Validation of previous work

According to Rathakrishnan [38], the prior work was performed at aspect ratios of 3:3, 3:2, and 3:1; an area ratio of 6.25; L/D ranging from 1 to 6; pressure ratios of 1.141, 1.295, 1.550, 1.707, and 2.458; and nozzle exit Mach numbers of 0.44, 0.62, 0.82, 0.91, and 1.0. However, in a prior publication by Rathakrishnan [38], the result from Figure 4 with NPR (P_{01}/P_a) 2.458 and models with control in the form of ribs with 3:2 and 3:3 aspect ratios was chosen to be compared to the current work. The simulation is supported by Rathakrishnan's [38] experimental work, which used five ribs positioned at equidistant intervals in the duct, as illustrated in Figure 3. The results of base pressure fluctuation with NPR of 2.458 and L/D ranging from 2 to 6 are obtained. The study is repeated to validate the numerical results of a model with control over different rib aspect ratios.

Figure 4 demonstrates the current and earlier studies' base pressure ratio data curves [38]. The experimental values were denoted by dotted lines, while the simulation results obtained using ANSYS Fluent were represented by straight lines. The present numerical analysis exhibited a percentage discrepancy of less than 10% compared to the previous experimental study. Consequently, the current work met the criteria for acceptability. The curves exhibited a consistent pattern, with each

point close to the subsequent one. As a result, based on the table and graph described before, the validation of the current work was successful.

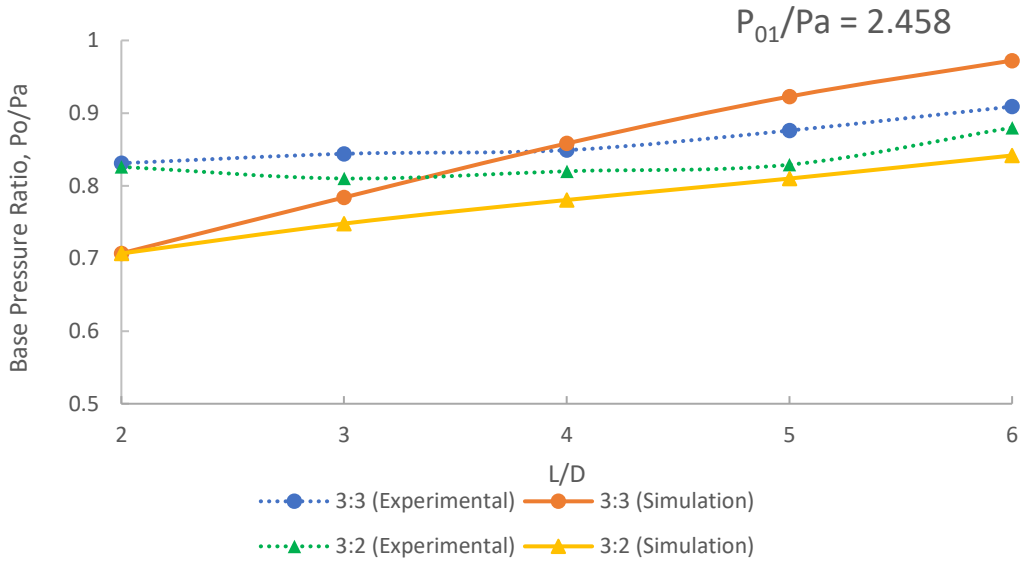

Fig. 4. Validation of previous work by Rathakrishnan [38]

3.6 Mesh Independence Study

Table 2 provides data from a mesh independence study, a crucial step in computational simulations to ensure that the results remain consistent regardless of the mesh refinement level. The element sizes range from the coarsest to the finest, with corresponding node and element counts for each mesh configuration. As the mesh becomes finer, the number of nodes and elements increases significantly, from 1,284 nodes and 1,145 elements in the coarsest mesh to 1,354,262 nodes and 1,351,303 elements in the finest mesh.

This study aims to determine the optimal mesh size for accurate simulations without unnecessary computational expense. The table shows a notable increase in nodes and elements as the mesh is refined. The coarsest mesh has relatively few nodes and elements, which means lower computational cost but potentially less accuracy. Conversely, the finest mesh offers the highest resolution at the expense of significant computational resources. The medium and fine meshes provide intermediate levels of refinement, offering a balance between accuracy and efficiency.

Based on the node and element numbers trends, the finest mesh will likely produce the most accurate results (Figure 5). However, continuing to refine the mesh beyond a certain point may offer diminishing returns in terms of accuracy while significantly increasing computational time. A critical assessment of this table would suggest that the "Fine" or "Finer" mesh configurations may represent the best balance between accuracy and computational efficiency. These configurations substantially increase nodes and elements compared to the medium meshes without reaching the computational expense of the finest mesh. If simulation results do not significantly change between the fine and finest meshes, further refinement to the finest mesh is unnecessary, as it would only increase computational time without added benefit. Thus, the fine or finer mesh sizes are likely the best choices for further simulation.

Table 2
Mesh independence study

Element size	Coarsest	Coarse	Medium 1	Medium 2	Fine	Finer	Finest
Nodes	1284	1933	7490	15240	124938	359022	1354262
Elements	1145	1777	7237	14895	124008	357492	1351303

Fig. 5. Results of mesh check

4. Results and Discussions

After the flow mechanics are understood completely, the base pressure results induced by the ribs should be analyzed when the shear layer is exhausted in a larger area duct. If the Mach number is less than unity, the boundary layer comes out of the nozzle, spreads out, and rejoins the larger duct. Given that the initial vortex is near the base and reasonably strong, one or more vortices will exist in the separated zone. We refer to it as the core vortex. It will act as a pump, transferring fluids from the base area to the edge of the boundary layer, where the main jet is situated. This pushing action will cause low pressure to form in the recirculation zone. However, because this vortex propagation is known to happen occasionally, the pushing action is too erratic. This chaotic pattern leads to variations in the base pressure. However, as the tests are conducted, it is evident that these base pressure variations are minor.

Consequently, we employ the mean base pressure values in our data evaluation. Because of the vortex desquamation's cyclicity, the extended image's entire flow pattern can be oscillatory. These oscillations can become highly severe regarding geometrical and inertia characteristics. The main factors influencing the strength of the central vortex at the base are the area ratio, Mach number, degree of expansion, and reattachment length.

This section discusses base pressure results for various rib locations, radius, duct lengths from L = 1D to 6D, and nozzle pressure ratio from 3 to 11.

Figure 6 shows a view of the converging-diverging nozzle with duct and quarter-circle rib for orientation one. The figure shows that the curved part faces the flow from the nozzle first, whereas the straight part of the rib is demonstrated towards the trailing edge.

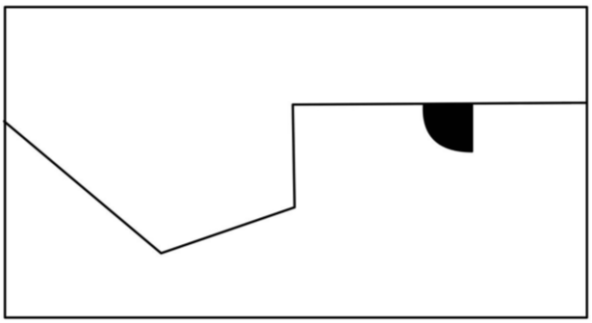

Fig. 6. A view of the C-D nozzle, enlarged duct, and quarter rib assembly

4.1 Base Pressure Results when Rib is Placed at 0.5D

The computed base pressure values are gauge pressure, and they are converted to absolute pressure by adding ambient pressure and are normalized by dividing absolute pressure by ambient pressure. The Mach number of the present study is 1.3. The nozzle pressure ratio (P0/Pa = NPR) needed for correct expansion is 2.77. The CFD simulations were done at the following NPRs in the range 3 to 11 in step 2, and the corresponding levels of expansion at these NPRs are 1.08, 1.8, 2.52, 3.25, and 3.97. From the range of the NPRs, it is evident that right from the NPR = 3, the nozzles are correctly expanded and under-expanded, and there is a progressive increase in the under-expansion level with an increase in the NPRs.

Figure 7(a) to Figure 7(f) show the base pressure results of the present study when the quarter rib is located at 11 mm (0.5D) from the base for NPRs ranging from 3 to 11 for rib radius from 1 mm, 2 mm, 3 mm, and 4mm. When we look at base pressure results for a duct size of 22 mm(1D), in the absence of the Rib as a passive control, the decreasing trend in the base pressure continues till NPR = 5; for NPR beyond five, the decreasing trend is arrested and base pressure is progressively increasing, and base pressure values are 55% of the ambient pressure. When passive control is employed with various radii in the range of 2mm, 3mm, and 4mm, there is a progressive increase in the base pressure values, and at the highest NPR of 11, the base pressure values are 2.2, 1.7, 0.9 times the ambient pressure. It is also seen that right from NPR = 3, there is a continuous linear rise in the base pressure. Such significant increases in the base pressure are attributable to excessive interactions of the waves at different NPRs, and the strength of the waves will vary with the rise in NPR, as seen in Figure 7(a).

We know that the reattachment point for the 22 mm duct size will be far away from the base compared to the 1D duct size, and it is insufficient for the flow to remain attached to the duct wall. This short duct size will not be attached to the wall of the pipe and is exposed to atmospheric pressure. Hence, these base pressure values are not considered when designing space vehicles/systems.

Figure 7(b) displays base pressure resulting from rib location at 11 mm from the base when duct size is 44 mm (i.e., L = 2D = 44mm) and the NPRs in the range from 3 to 11. The fundamental variations for this duct length L = 2D and L = 1D are: the downward trends in the base pressure seen for duct length L = 1D are not to be seen, and that trend is absent. There is a considerable increase in the base pressure values when control is not employed. However, when ribs of radii 1 mm, 2 mm,

3 mm, and 4 mm are used, the control rib will interact with the waves formed at the nozzle exit, and the same will hit the wall and be reflected, resulting in a considerable increase in the base pressure. The largest rib radius of the current study results in a maximum increase in the base pressure as it blocks the main flow and transfers sufficient mass toward the base region. Besides, the base pressure for rib radii 2 mm to 3 mm maintains increasing trends and increases 70% and 30% more than atmospheric pressure.

Figures 7(c) to 7(f) show similar trends as was seen for lower duct lengths, except for a slight variation in the magnitude of the base pressure. These subtle variations are attributed to the changes in the duct lengths where the impact of the ambient pressure is at its lowest levels.

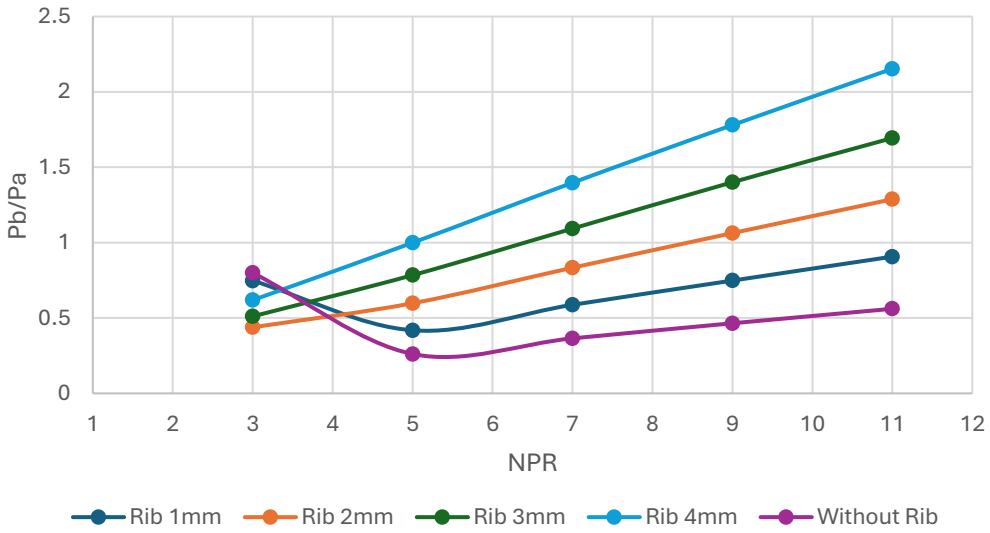

(a) L/D = 1

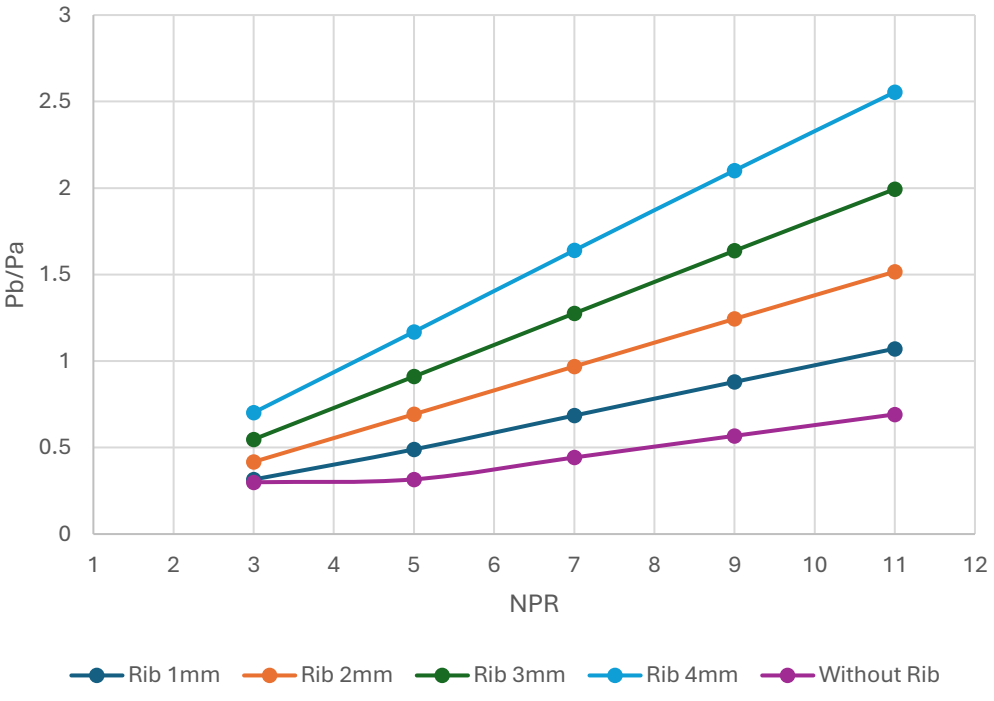

(b) L/D = 2

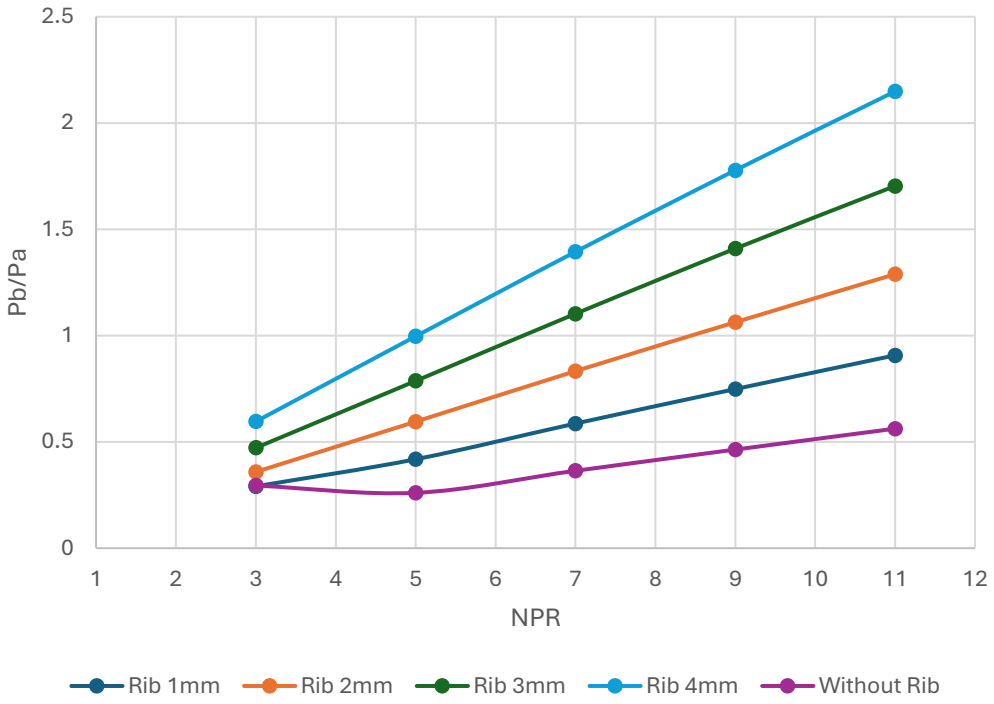
2.5
2
1.5
1
0.5
0
Pb/Pa
1
2
3
4
5
6
7
8
9
10
11
12
NPR
Rib 1mm
Rib 2mm
Rib 3mm
Rib 4mm
Without Rib

(c) L/D = 3

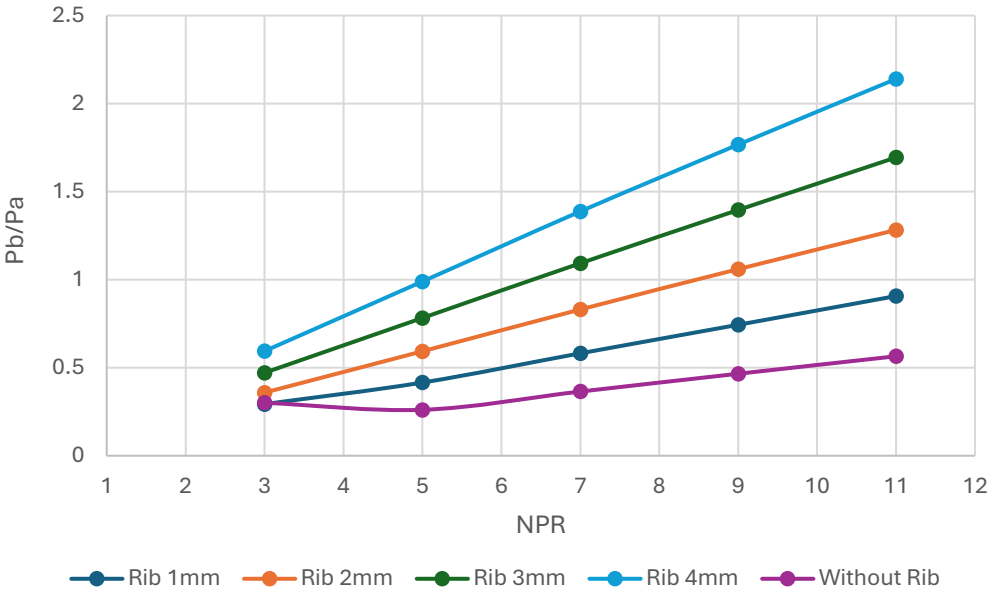
2.5
2
1.5
1
0.5
0
Pb/Pa
1
2
3
4
5
6
7
8
9
10
11
12
NPR
Rib 1mm
Rib 2mm
Rib 3mm
Rib 4mm
Without Rib

(d) L/D = 4

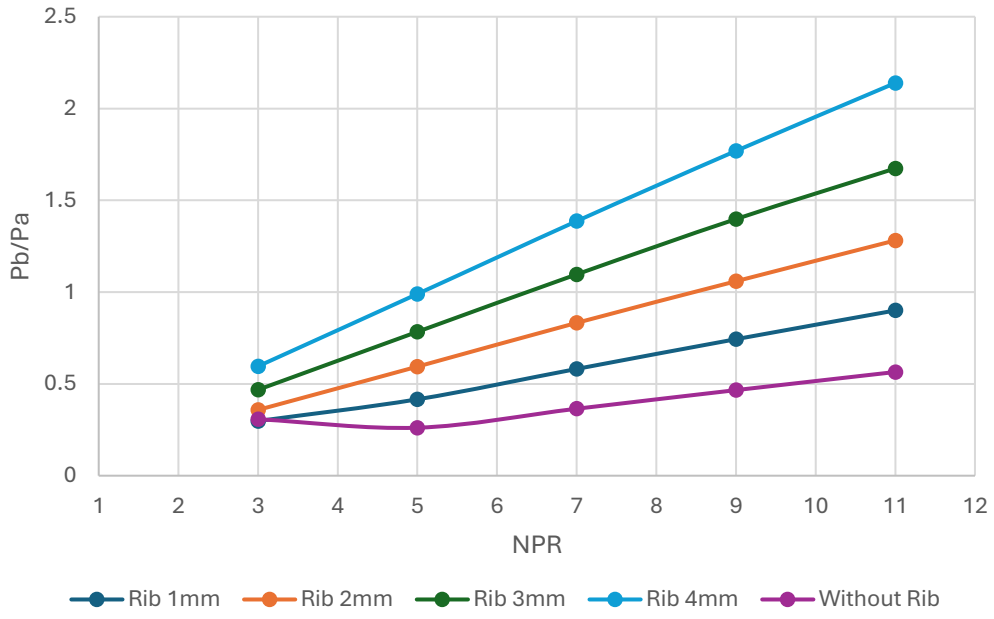

(e) L/D = 5

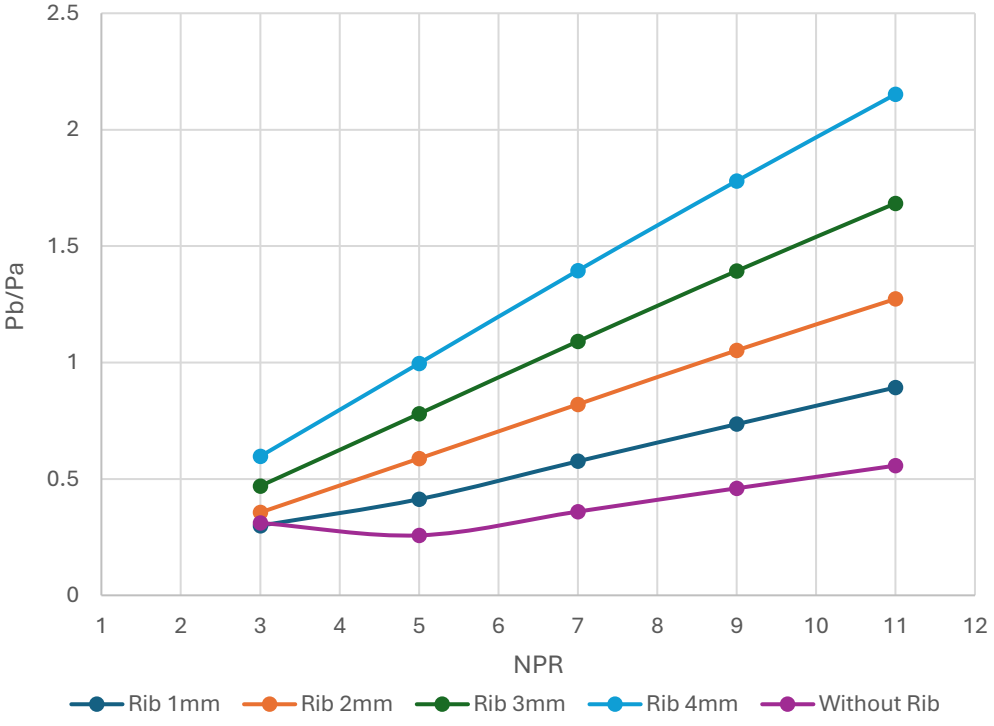

(f) L/D = 6

Fig. 7. Base Pressure Vs. NPR for various duct lengths

4.2 Base Pressure Results when Rib is Placed at 1D

Figure 8(a) to Figure 8(e) depict the base pressure resulting from this study when ribs of radii 1 mm, 2 mm, 3 mm, and 4 m are placed at 1D (i.e., 22 mm) from the base for various duct sizes L = 44 mm to 132 mm for NPRs in the range from 3 to 11. From Figure 8(a), it is seen that base pressure values in the absence of the Rib and when 1 mm rib is located at 1D location both have nearly the same values except at NPR = 3, this is remarkably different from the previous case when ribs were placed 11 mm from the base. This trend can be due to the change in the rib location, and the minimum duct length is 44 mm instead of 22 mm. This pattern is an outcome of duct-size rib location

with the same level of expansion. However, when we look at the base pressure results for rib radii 2 mm, 3 mm, and 4 mm, their values are 0%, 55%, and 120%, respectively, more than the ambient pressure. For a 2 mm rib radius, the base pressure equals the atmospheric pressure. Hence, a rib radius of 2 mm may be the right choice if the end-user wants to increase the base pressure to equal the ambient pressure.

Similar trends in base pressure are seen for higher duct lengths in the range 3D, 4D, 5D, and 6D, except that for more considerable duct lengths, namely L = 5D and 6D, the magnitude of the base pressure is marginally decreased. This reduction in the base pressure is due to the significant duct length; the influence of ambient pressure is less compared to the smaller duct exposed to the ambient atmospheric pressure.

Hence, the end user can decide on the rib radius while using the technology, depending on the mission requirements.

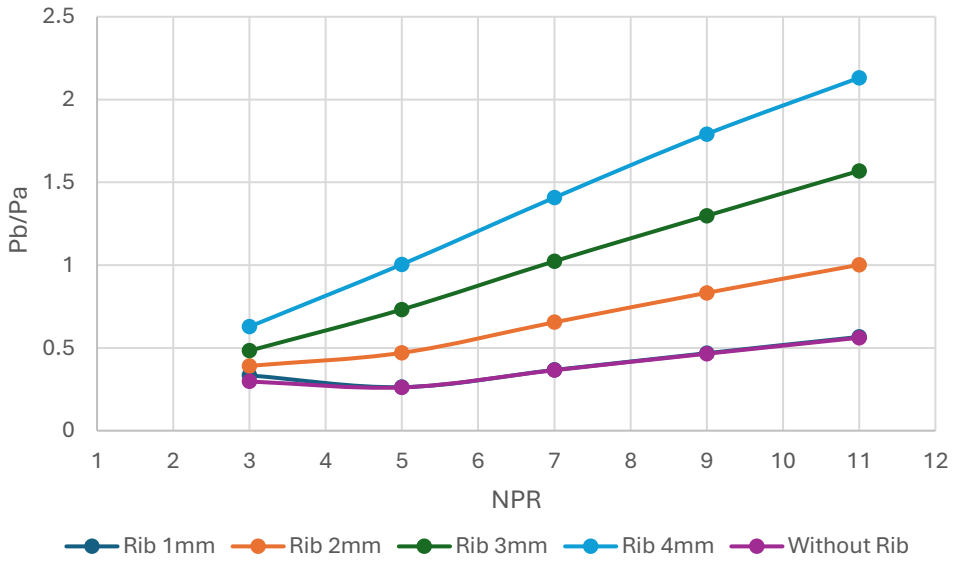

(a) L/D = 2

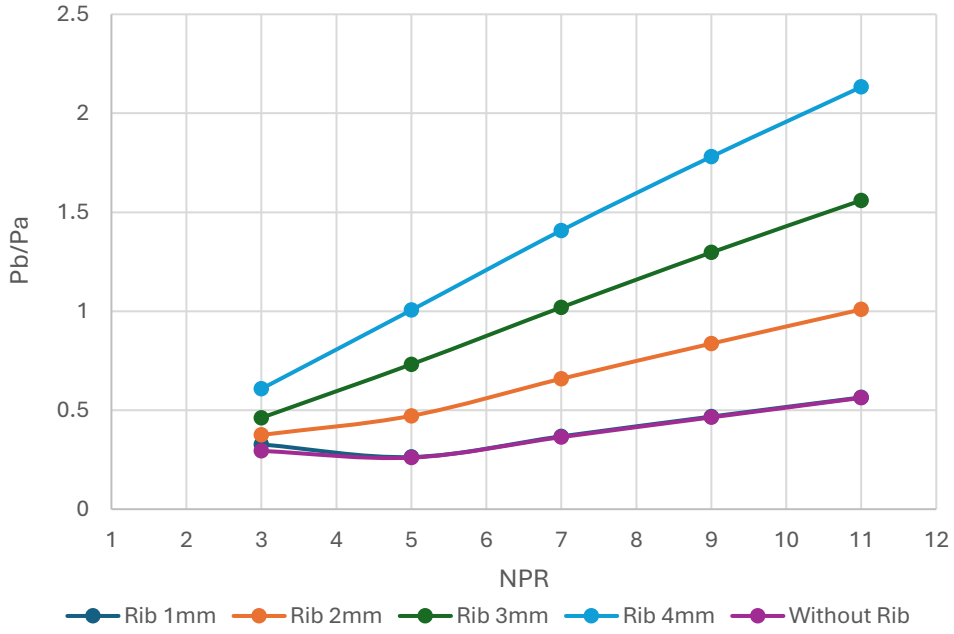

(b) L/D = 3

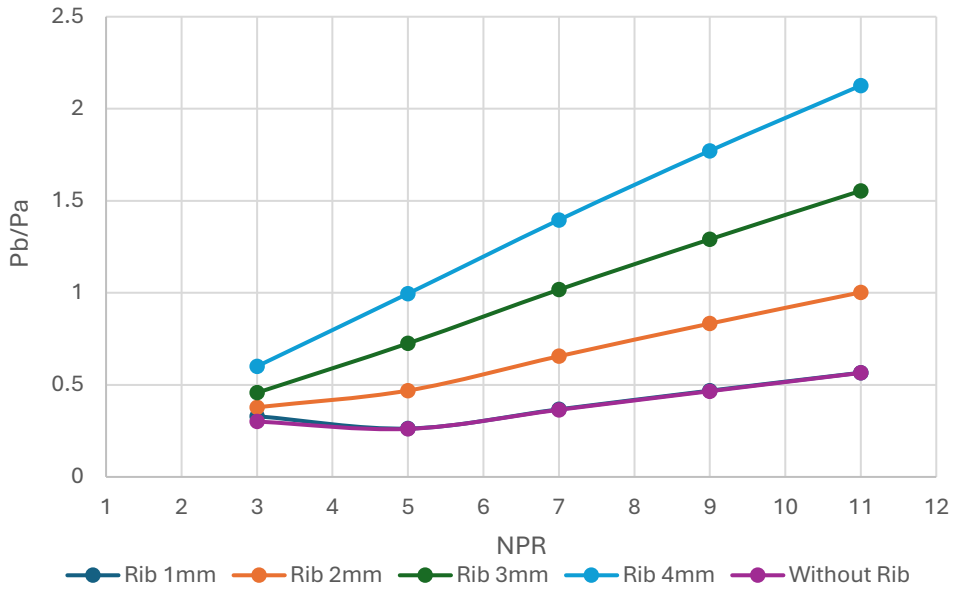
2.5
2
1.5
1
0.5
0
Pb/Pa
1
2
3
4
5
6
7
8
9
10
11
12
NPR
Rib 1mm
Rib 2mm
Rib 3mm
Rib 4mm
Without Rib

(c) L/D = 4

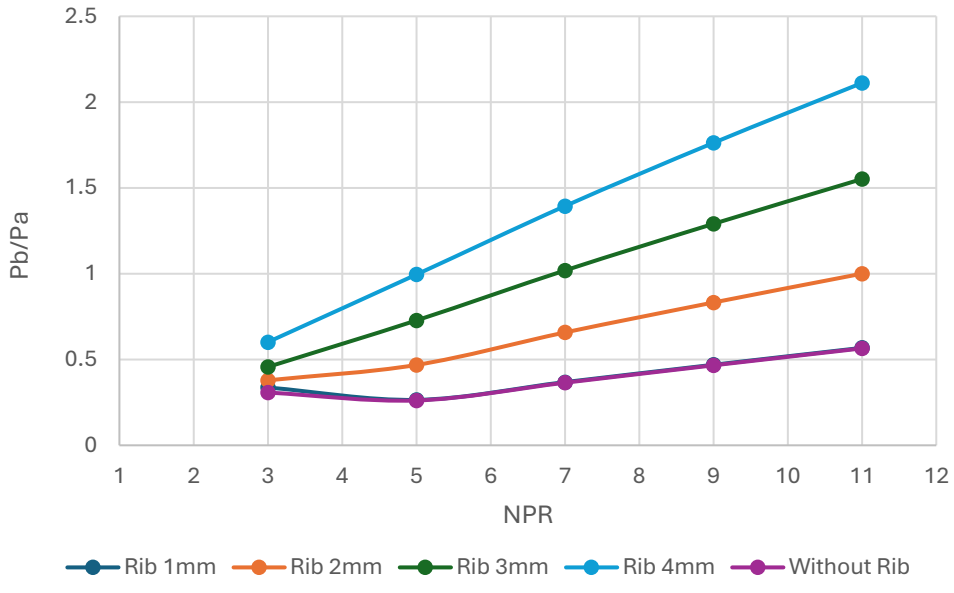
2.5
2
1.5
1
0.5
0
Pb/Pa
1
2
3
4
5
6
7
8
9
10
11
12
NPR
Rib 1mm
Rib 2mm
Rib 3mm
Rib 4mm
Without Rib

(d) L/D = 5

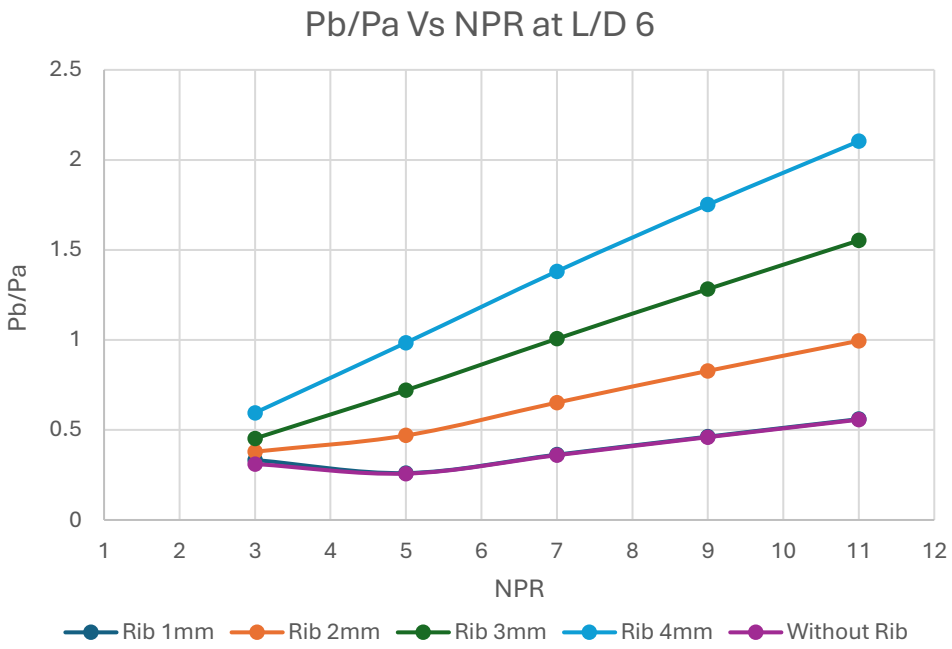

(e) L/D = 6

Fig. 8. Base Pressure Vs. NPR for various duct lengths

4.3 Base Pressure Results when Rib is Placed at 1.5D

Figure 9(a) to Figure 9(e) shows findings of this study when passive control in the form of a quarter circle rib is placed at 33 mm from the base inside the duct for various rib radii in the range from 1 mm to 4 mm and NPRs in the range from 3 to 11. Figure 9(a) depicts the outcome of this study when the duct size is 44 mm (i.e., 2D); from the figure, it is seen that there is a considerable increase in the base pressure values in comparison to the previous case where a rib was located at 22 mm from the base. For three rib radii, the base pressure is 1.2, 1.95, and 2.75 times the ambient pressure, whereas base pressure in the absence of a rib and with a 1 mm rib remains the same. This trend is because the reattachment point is expected to be around 44 mm to 66 mm from the base. That may be one of the reasons that base pressure increases with the shift of the Rib towards the downstream.

Similar results are found when the size is increased to 66 mm from 44 mm, as seen in Figure 9(b). With a further increase in the duct length, there is a marginal decrease in the base pressure values (Figure 9(c) to Figure 9(e)). This variation in the base pressure is attributed to the suction created by the larger duct size, and ambient pressure fails to influence the flow inside the duct.

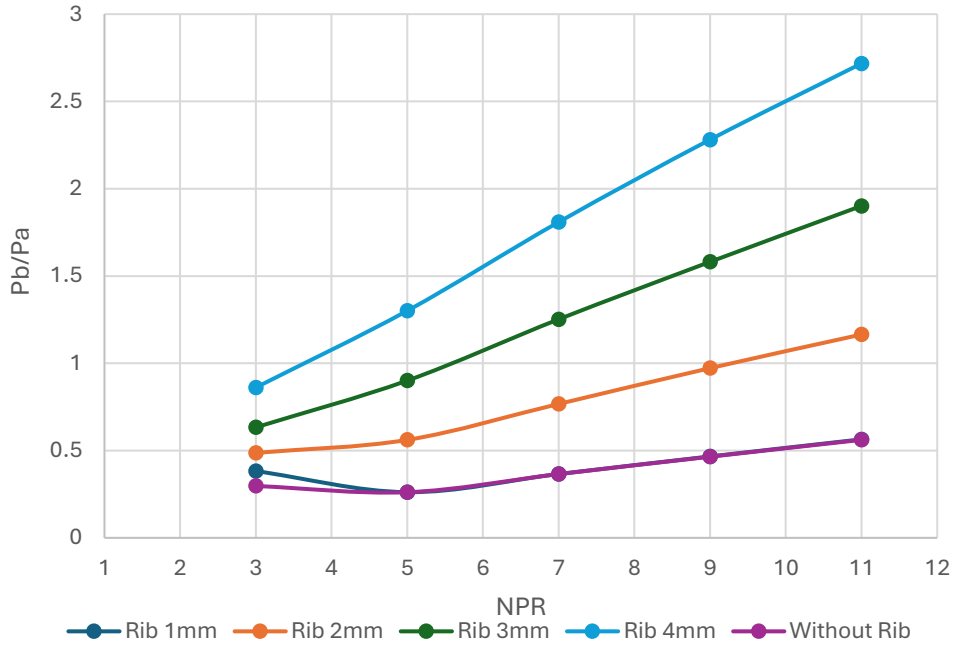
Pb/Pa
NPR
Rib 1mm
Rib 2mm
Rib 3mm
Rib 4mm
Without Rib

(a) L/D = 2

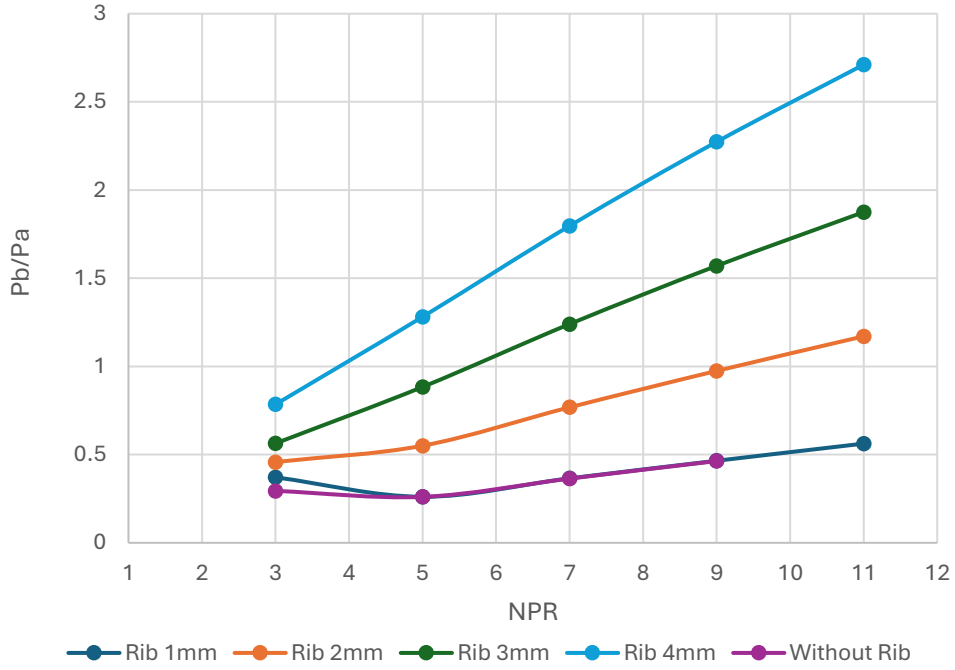
Pb/Pa
NPR
Rib 1mm
Rib 2mm
Rib 3mm
Rib 4mm
Without Rib

(b) L/D = 3

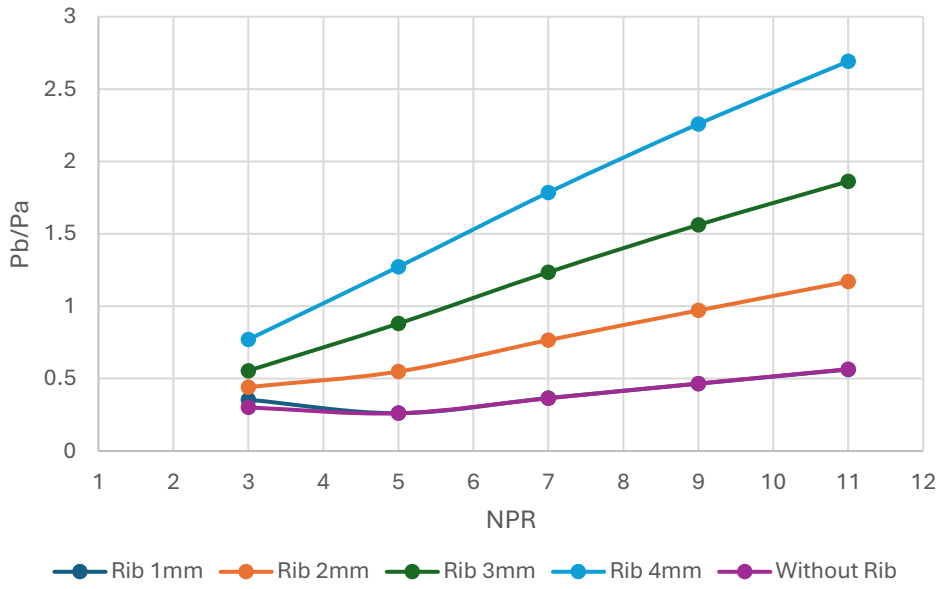
Pb/Pa
NPR
Rib 1mm
Rib 2mm
Rib 3mm
Rib 4mm
Without Rib

(c) L/D = 4

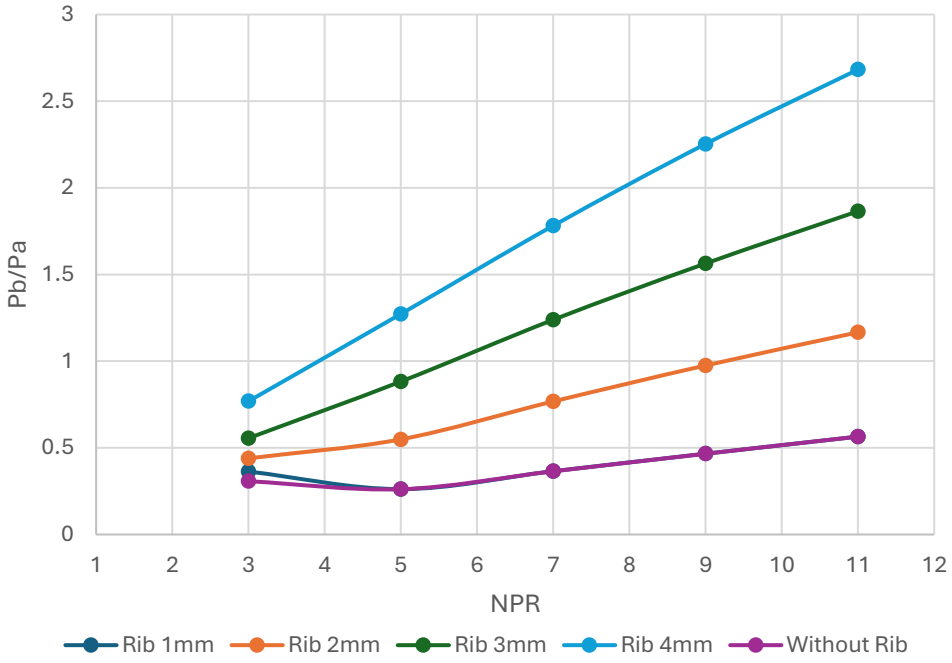
Pb/Pa
NPR
Rib 1mm
Rib 2mm
Rib 3mm
Rib 4mm
Without Rib

(d) L/D = 5

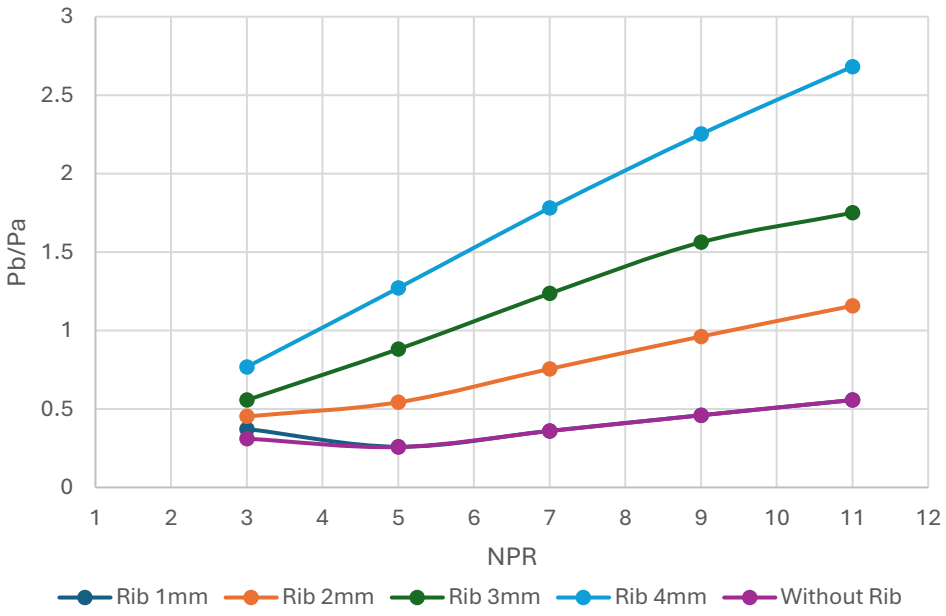

(e) L/D = 6

Fig. 9. Base Pressure Vs. NPR for various duct lengths

4.4 Base Pressure Results when Rib is Placed at 2D

When the quarter ribs of radii in the range from 1 mm to 4 mm are employed at 44 mm from the base for duct lengths in the range from L = 1D to 6D for various nozzle pressure ratios in the range from 3 to 11, are shown in Figure 10(a) to Figure 10(d). As seen in Figure 10(a), there is a considerable rise in the base pressure values due to the shift in the rib location towards the trailing edge of the duct. Base pressure values are 30%, 130%, 215%, and 325% of the atmospheric pressure values when ribs of radii 1 mm, 2 mm, 3 mm, and 4 mm are located at 44 mm from the base. As discussed earlier, in this case, a rib of 1 mm radius and the base pressure values are identical without a rib. That implies that a 1 mm radius rib cannot influence the flow field inside the duct and remains the same as was found without a rib. The physics of the flow may be understood like this. When the Rib of 1 mm radius is placed at 44 mm from the base of the duct, some mass is drawn from the main flow to transfer towards the base of the duct. Still, it gets neutralized by the interaction of the expansion waves, and in this process, it becomes counterproductive; hence, the base pressure remains constant. Nevertheless, when we look at base pressure results for rib radii from 2 mm to 4 mm, control becomes very effective, and there is a significant increase in the base pressure, as seen in Figure 10(c) to Figure 10(d). However, for larger duct sizes in the range from L = 4D to 6D, there is a marginal reduction in the base pressure, and this slight decrease in the base pressure is attributable to the fact that the duct size is increased significantly and ambient pressure is unable to impact the flow inside the duct.

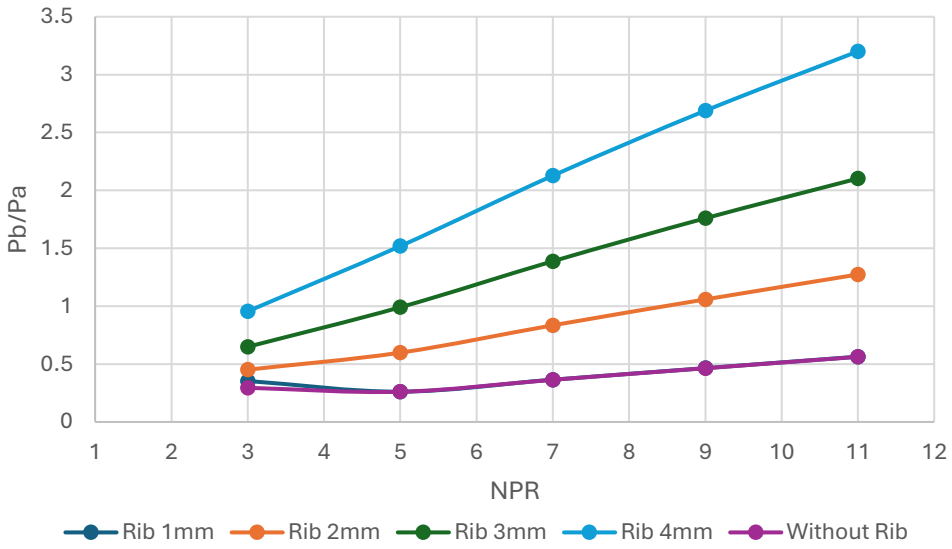

(a) L/D = 3

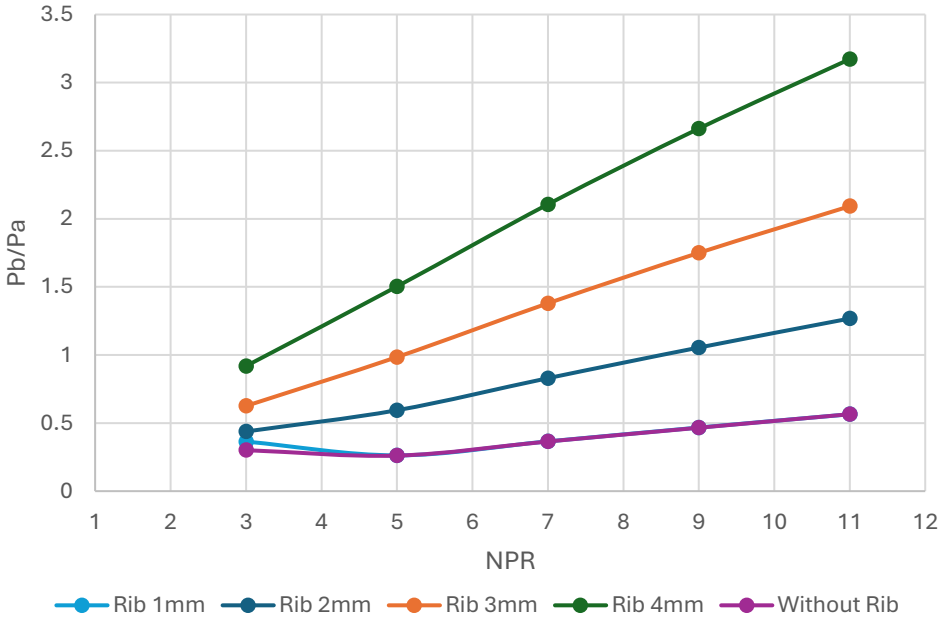

(b) L/D = 4

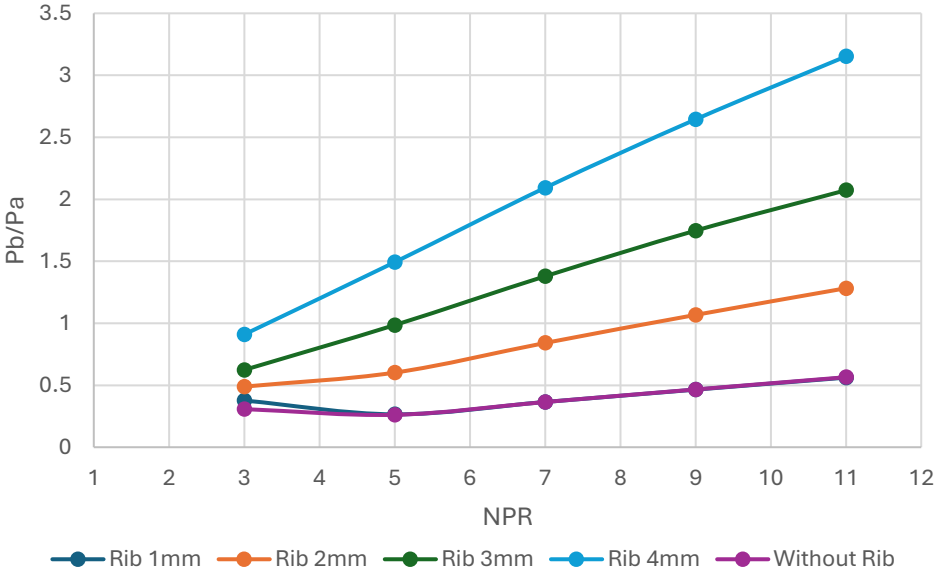

(c) L/D = 5

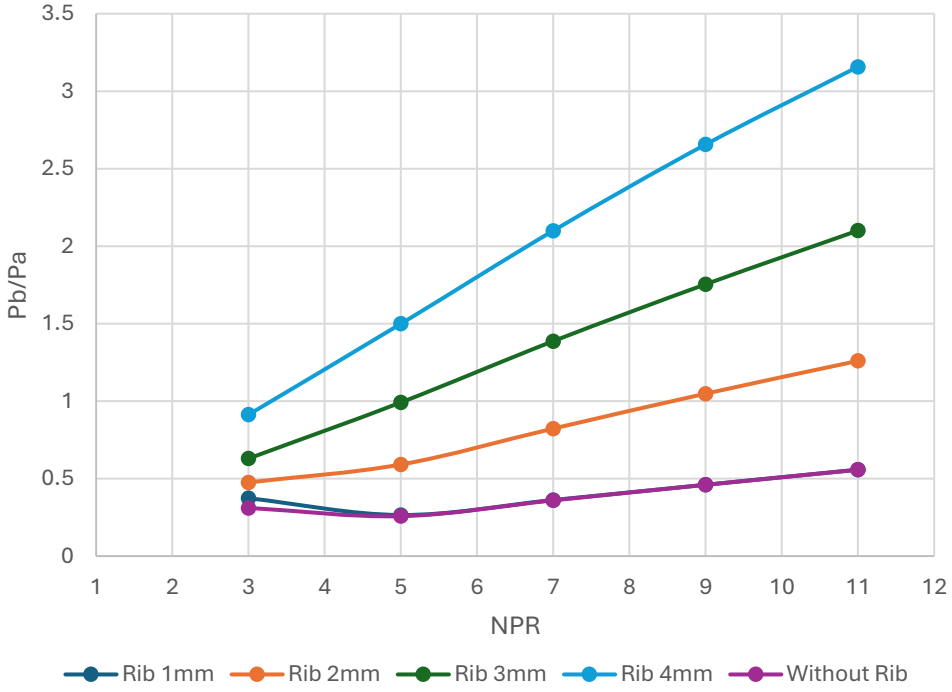

(d) L/D = 6

Fig. 10. Base Pressure Vs. NPR for various duct lengths

4.5 Base Pressure Results when Rib is Placed at 3D

The findings of this study are shown in Figure 11(a) to Figure 11(c) when ribs of various radii are located at 66 mm from the base for nozzle pressure ratios in the range from 3 to 11 and duct sizes L = 4D to 6D. Because of the further shift of the Rib located towards the trailing edge, there is a significant increase in the base pressure for all three radii of the ribs in the range from 2mm to 4 mm. and the base pressure results for 1 mm rib radius and in the absence of the control remains the same as it happened for other rib positions. A 3.8 times increase in base pressure is achieved for a 4 mm rib radius. However, this increase is 245% and 145% for rib radii 3 mm and 2mm. These changes in the base pressure can be due to the rib positioning near the reattachment point, resulting in the maximum gain in the base pressure. As discussed earlier, for the highest duct sizes L = 5D and 6D, there is a slight decrease in the base pressure values as for such considerable duct length, ambient pressure will not have any role to play in influencing the flow inside the duct, as there is sufficient duct length available to the flow to negate the ambient pressure impact.

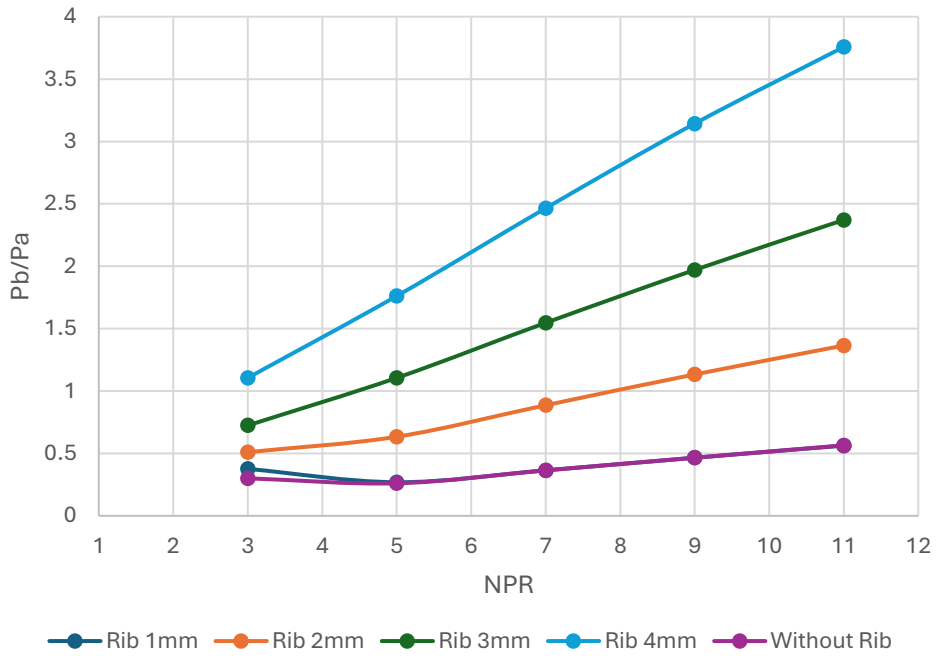
Pb/Pa
NPR
Rib 1mm
Rib 2mm
Rib 3mm
Rib 4mm
Without Rib

(a) L/D = 4

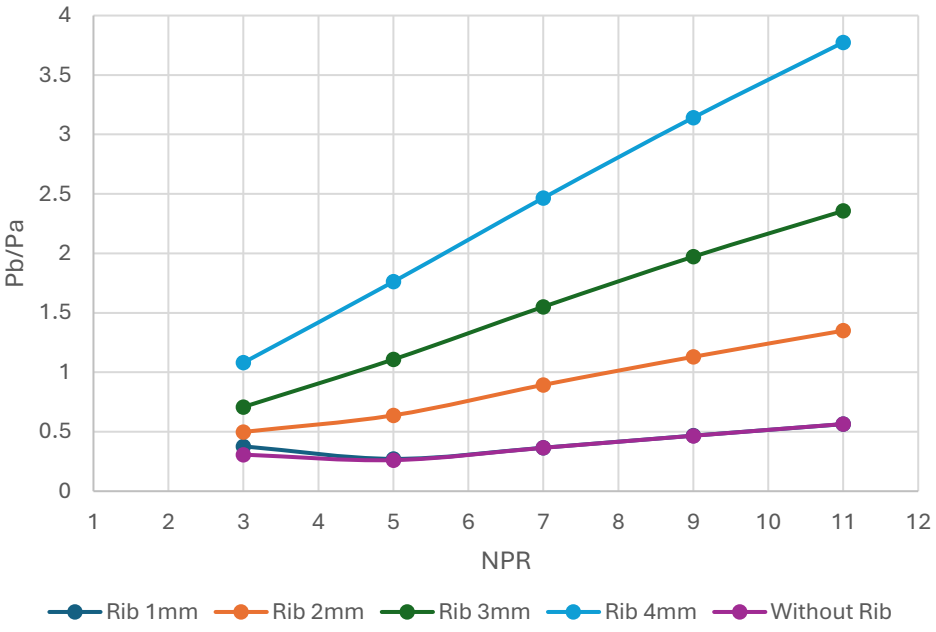
Pb/Pa
NPR
Rib 1mm
Rib 2mm
Rib 3mm
Rib 4mm
Without Rib

(b) L/D = 5

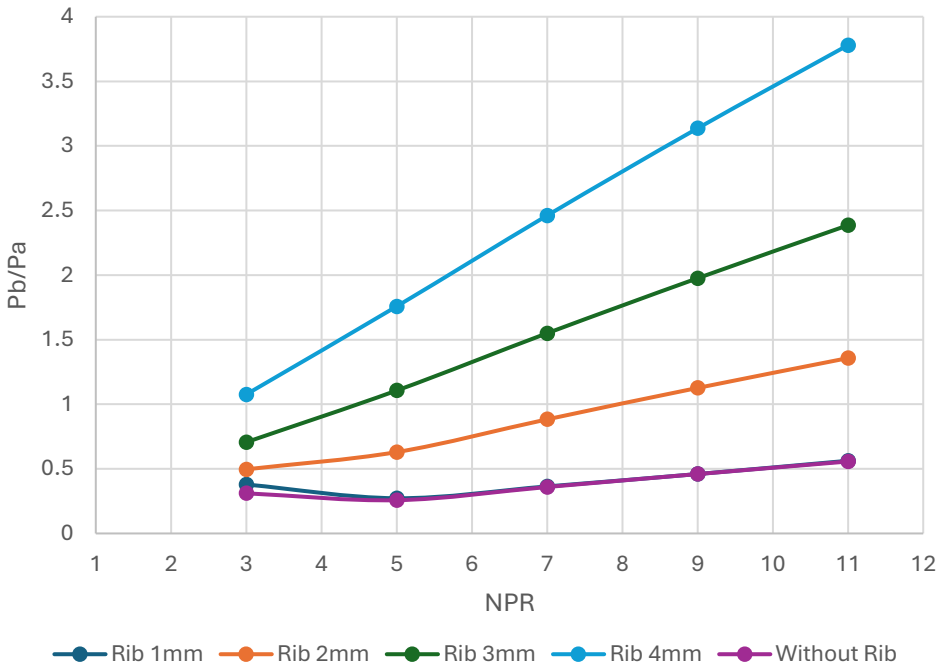

(c) L/D = 6

Fig. 11. Base Pressure Vs. NPR for various duct lengths

4.6 Pressure Contours

Figure 12(a) to Figure 12(d) demonstrates pressure contours at a rib location of 1.5D, specifically for a length-to-diameter (L/D) ratio of 6 and a nozzle pressure ratio (NPR) of 5. These figures reflect the outcomes of various rib radii employed as passive control strategies to regulate base pressure within the duct. When examining the 1 mm rib radius, the contours reveal that this size is inadequate for effectively enhancing the base pressure. The flow seems less affected by the Rib, thus displaying relatively weak control over the turbulent expansion. In contrast, the 2 mm rib radius presents contours that indicate improved control, contributing to a noticeable increase in base pressure compared to 1 mm. In the case of a 3 mm rib radius, this variant shows further advancements in pressure distribution, effectively increasing base pressure. The contours imply that the flow field is managed more efficiently, enhancing aerodynamic performance. Finally, the 4 mm rib radius demonstrates the most substantial enhancement in base pressure among the four examined radii. The contours signify a highly regulated flow, marked by a significant rise in base pressure, which is particularly effective for the specified duct configuration.

Figure 12(a) to Figure 12(d) illustrate that an increase in rib radius from 1 mm to 4 mm progressively enhances control over base pressure, optimizing the aerodynamic characteristics of the flow within the duct. However, the 1 mm rib is inadequate; the 2 mm, 3 mm, and 4 mm ribs prove effective. However, the 4 mm rib is the most impactful.

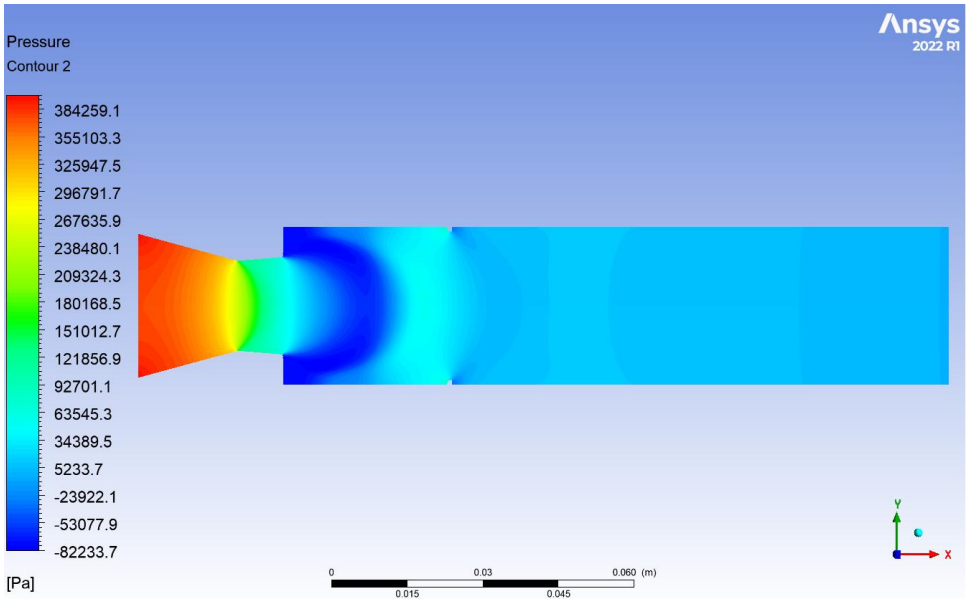
Ansys
2022 R1
Pressure
Contour 2
384259.1
355103.3
325947.5
296791.7
267635.9
238480.1
209324.3
180168.5
151012.7
121856.9
92701.1
63545.3
34389.5
5233.7
-23922.1
-53077.9
-82233.7
[Pa]
0
0.03
0.060 (m)
0.015
0.045
Y
X

(a) 1 mm

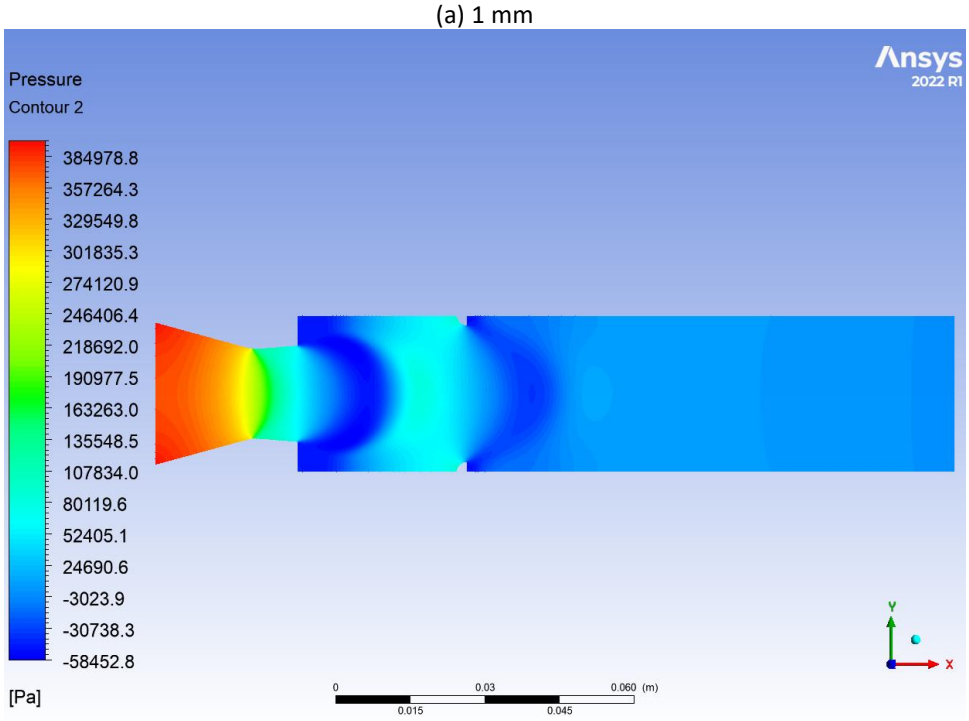
Ansys
2022 R1
Pressure
Contour 2
384978.8
357264.3
329549.8
301835.3
274120.9
246406.4
218692.0
190977.5
163263.0
135548.5
107834.0
80119.6
52405.1
24690.6
-3023.9
-30738.3
-58452.8
[Pa]
0
0.03
0.060 (m)
0.015
0.045
Y
X

(b) 2 mm

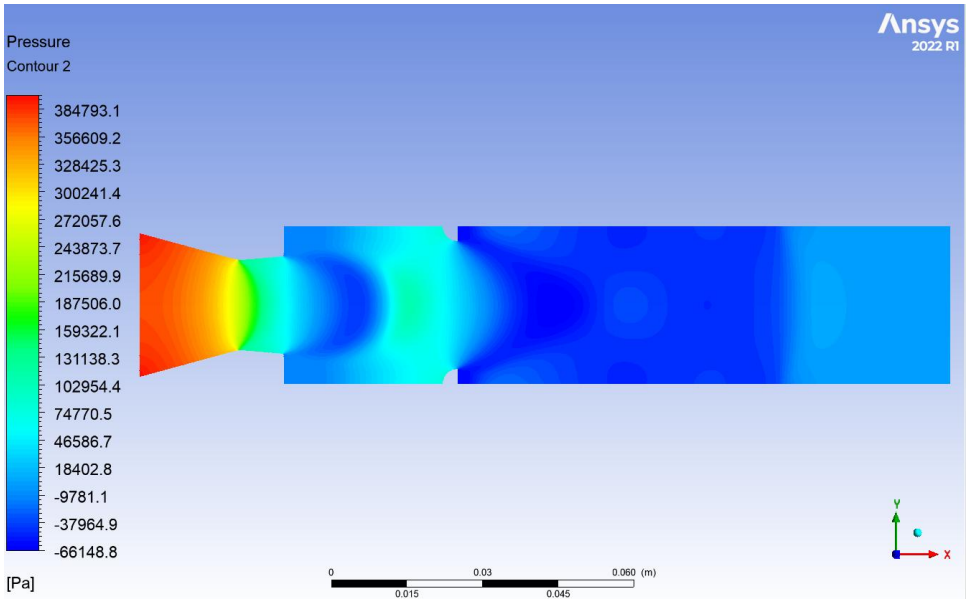

(c) 3 mm

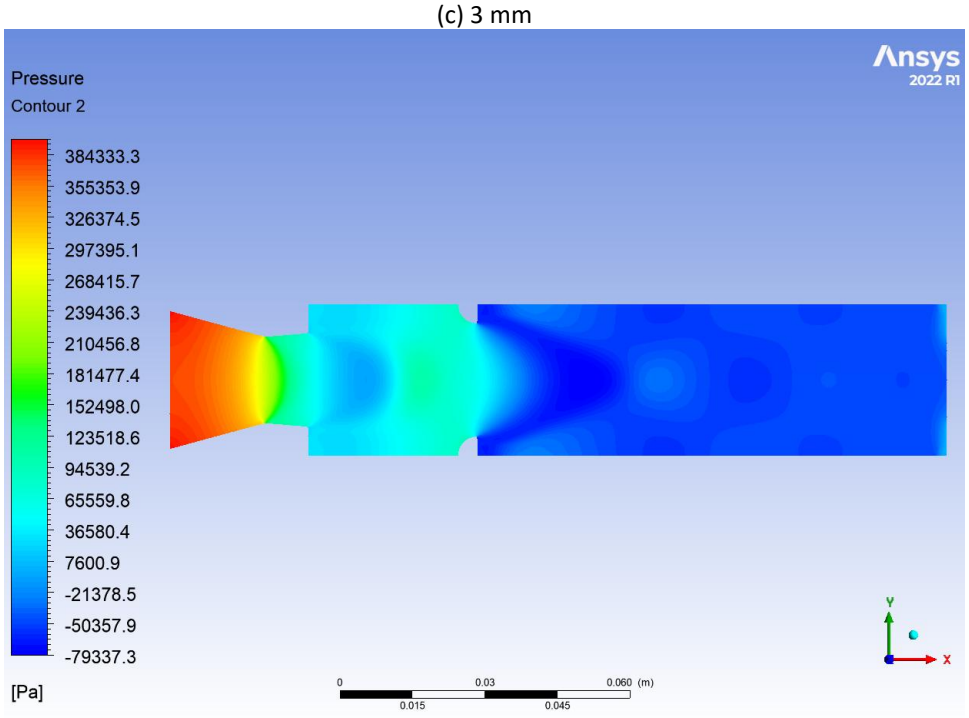

(d) 4 mm

Fig. 12. Pressure Contours for L/D = 6, NPR = 5 and at 1.5D location

4.7 Velocity Contours

Figure 13(a) to Figure 13(d) show the velocity contours corresponding to a particular configuration, specifically at a duct length-to-diameter ratio (L/D) of 6, a nozzle pressure ratio (NPR) of 5, and a location of 1.5D along the duct. These figures representing varying rib radii illustrate the contours for quarter ribs with radii of 1 mm, 2 mm, 3 mm, and 4 mm.

In the case of the 1 mm rib radius, this contour seemingly indicates a minimal effect on base pressure, as the accompanying text suggests that such ribs are insufficient to regulate base pressure effectively. Conversely, the 2 mm rib radius demonstrates a noticeable improvement in flow characteristics, resulting in enhanced flow management and increased base pressure. Furthermore, the 3 mm rib radius reveals an additional optimization in flow dynamics, contributing positively to

base pressure values. Finally, the 4 mm rib radius manifests the most noticeable effect among the configurations, significantly augmenting flow characteristics while concurrently sustaining elevated base pressure levels.

The transition from 1 mm to 4 mm rib radii elucidates how augmented rib dimensions influence the flow dynamics. Notably, larger rib radii (spanning from 2 mm to 4 mm) are incredibly proficient at regulating base pressure, as they adeptly manage reattachment and turbulence, surpassing the efficacy of the 1 mm rib. This observation underscores the critical importance of rib geometry in passive control mechanisms aimed at optimizing aerodynamic performance.

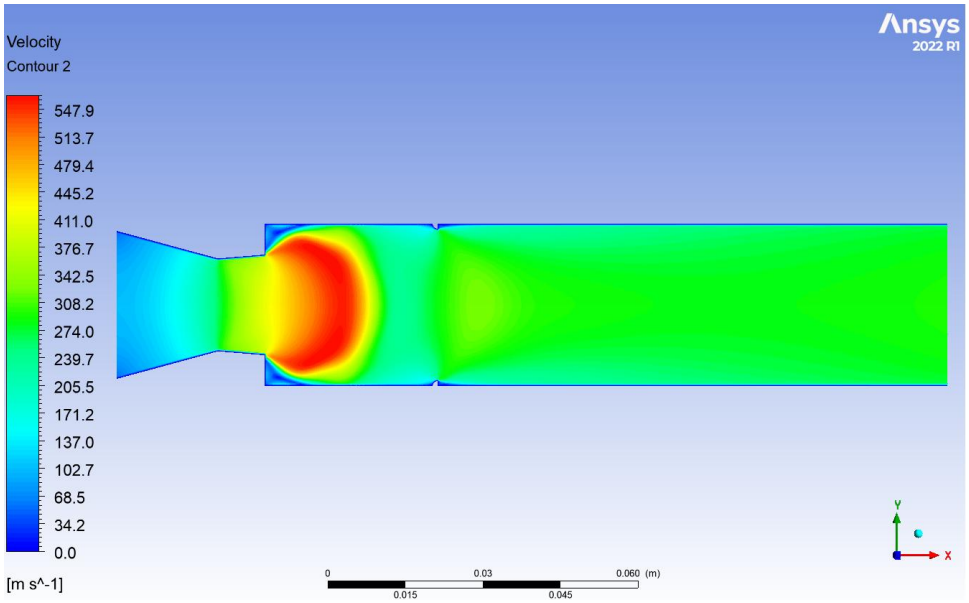

(a) 1 mm

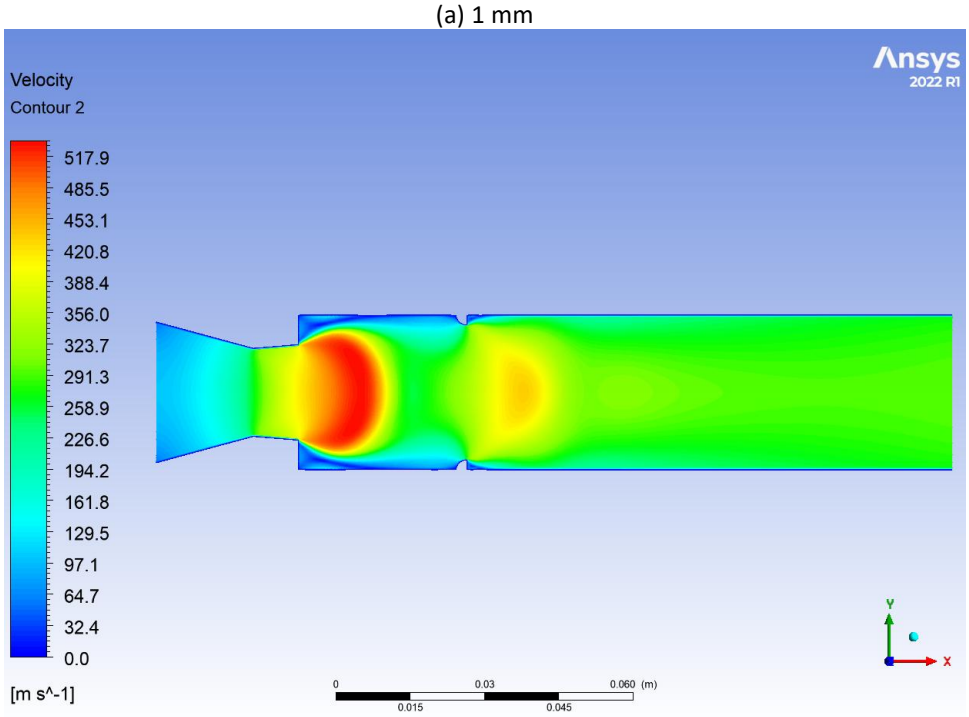

(b) 2 mm

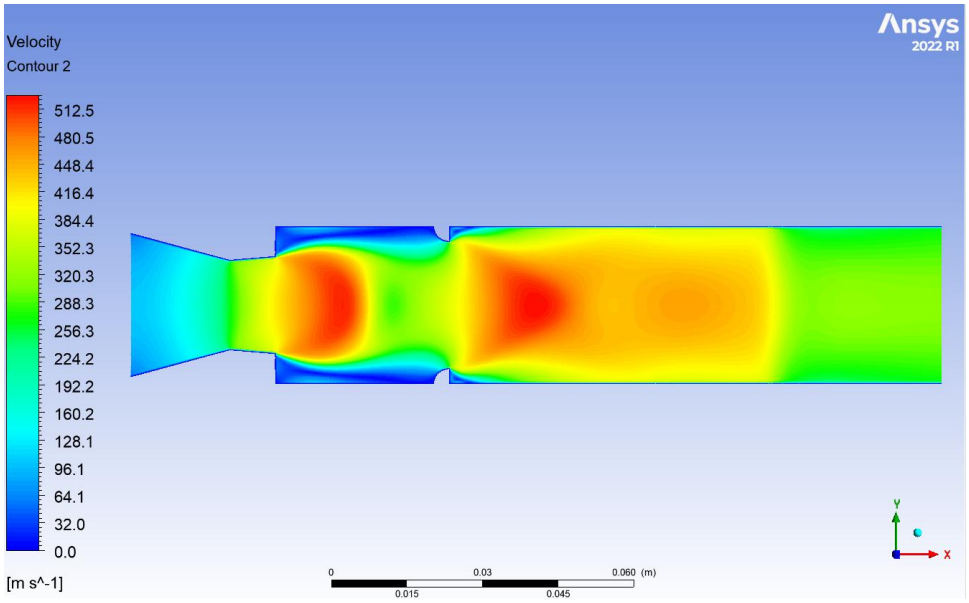

(c) 3 mm

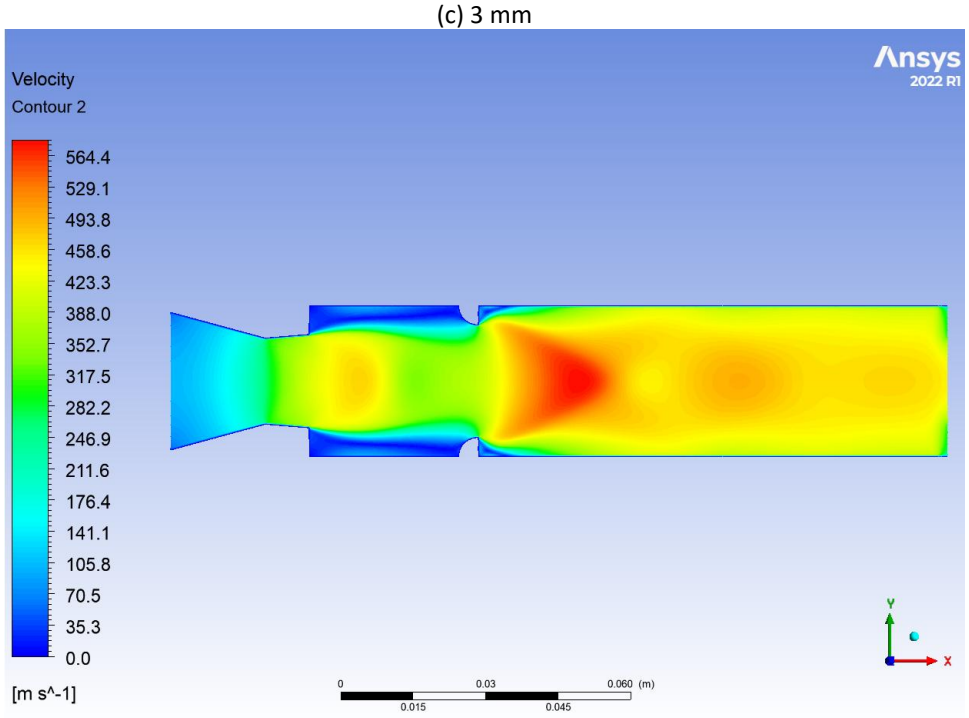

(d) 4 mm

Fig. 13. Velocity Contours for L/D = 6, NPR = 5 and at 1.5D location

4.8 Velocity Streamlines

Figure 14(a) to Figure 14(d) illustrate velocity streamlines within a duct characterized by a length-to-diameter ratio (L/D = 6) alongside a nozzle pressure ratio (NPR = 5) observed at the 1.5D position downstream. The behavior of the streamlines likely reveals the extent to which Rib radii will impact flow reattachment and turbulence within the expanded duct region; this presents patterns intimately linked to each specific rib size. The findings underscore the importance of rib dimensions in regulating base pressure because more prominent ribs (ranging from 2 mm to 4 mm) demonstrate greater efficacy at particular duct lengths.

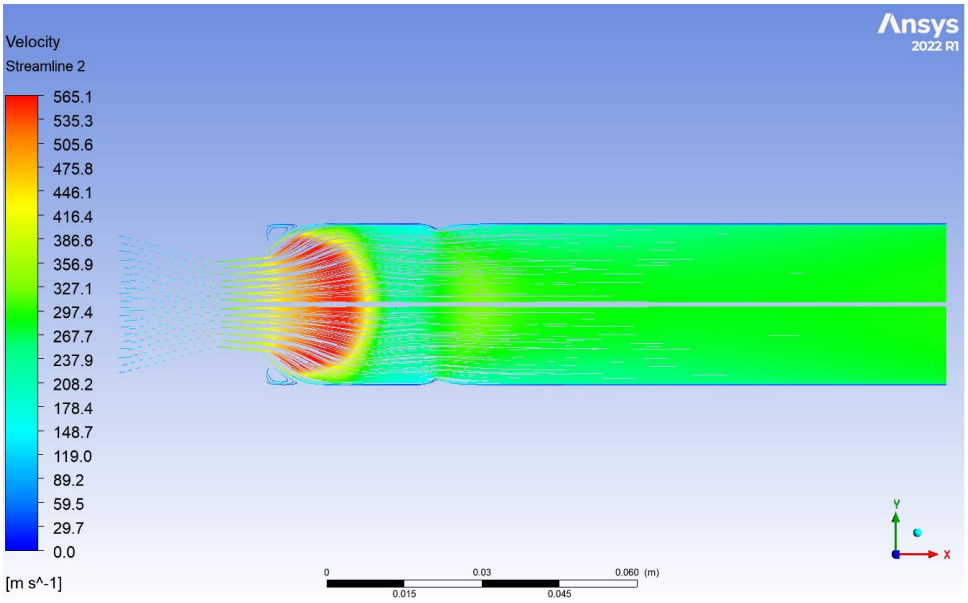
Ansys
2022 R1
Velocity
Streamline 2
565.1
535.3
505.6
475.8
446.1
416.4
386.6
356.9
327.1
297.4
267.7
237.9
208.2
178.4
148.7
119.0
89.2
59.5
29.7
0.0
[m s^-1]
0
0.03
0.060 (m)
0.015
0.045
Y
X

(a) 1 mm

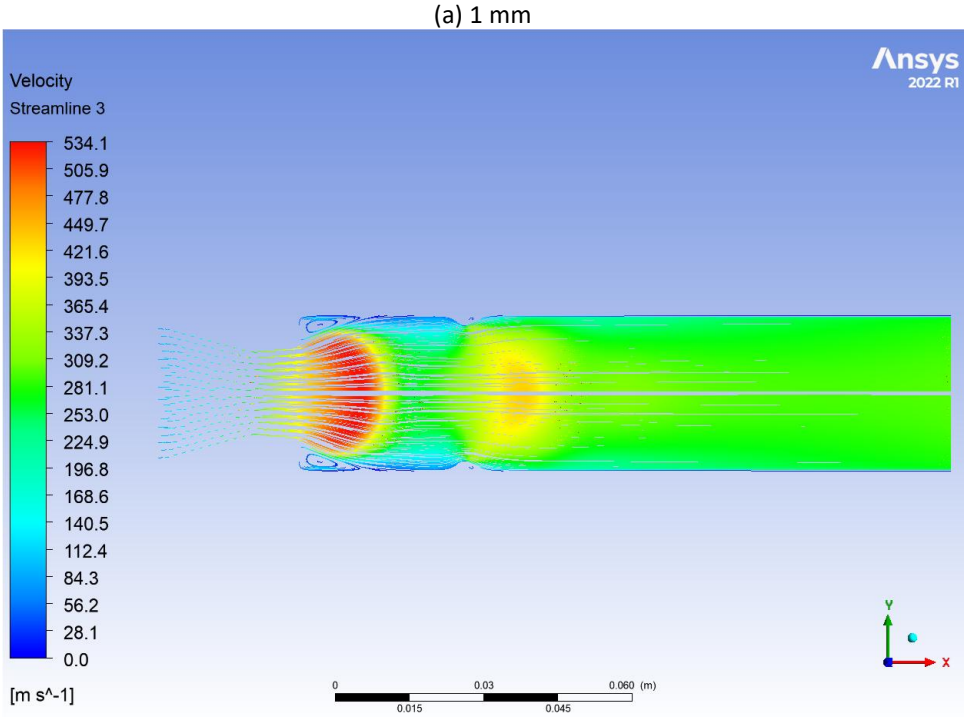
Ansys
2022 R1
Velocity
Streamline 3
534.1
505.9
477.8
449.7
421.6
393.5
365.4
337.3
309.2
281.1
253.0
224.9
196.8
168.6
140.5
112.4
84.3
56.2
28.1
0.0
[m s^-1]
0
0.03
0.060 (m)
0.015
0.045
Y
X

(b) 2 mm

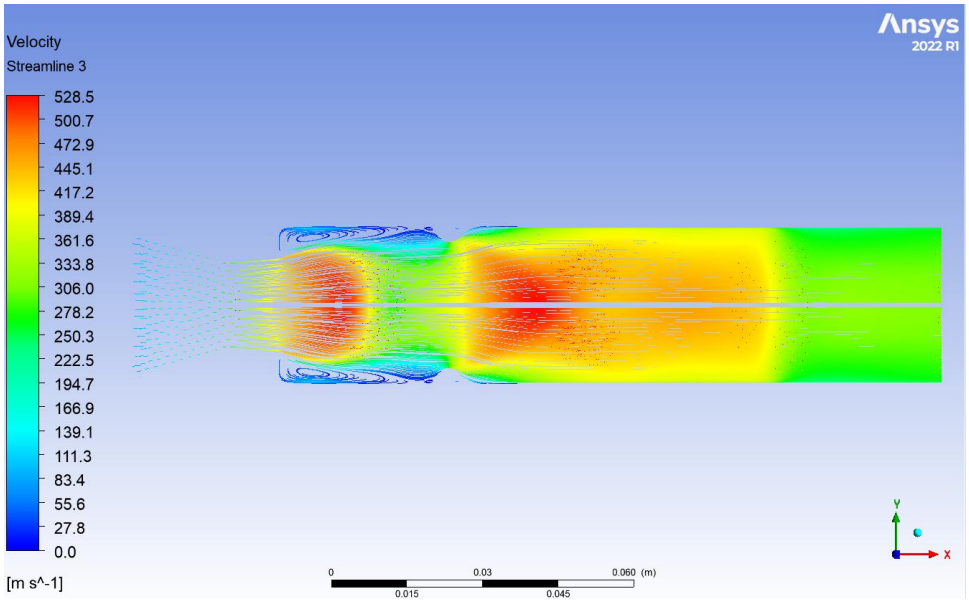

(c) 3 mm

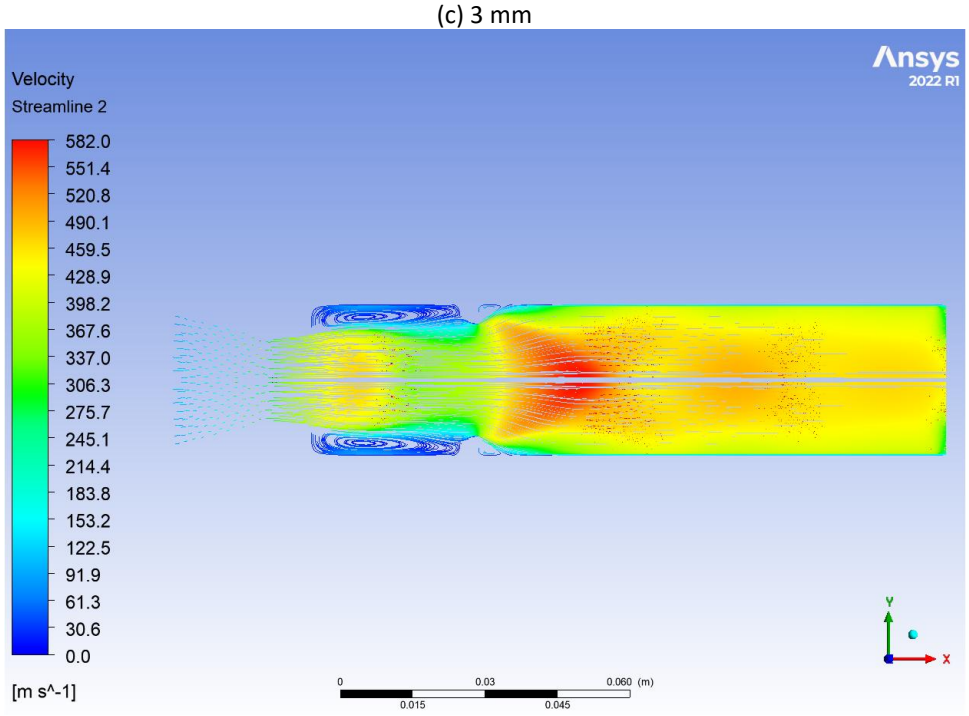

(d) 4 mm

Fig. 14. Velocity Streamlines for L/D=6, NPR=5 and at 1.5D location

5. Conclusion

Based on the above discussions, we may conclude that the base pressure values for a 1mm rib radius and in the absence of passive are the same as the Rib with a 1 mm radius is unable to make any impact in the flow field of the duct and hence it is ineffective. Thus, the quarter circle of 1 mm radius is considered inadequate, and the base pressure with and without control is nearly the same. Hence, this 1 mm radius is ineffective and should not be used unnecessarily; it adds additional weight to the system without any meaningful advantages. However, ribs with radii 2 mm, 3 mm, and 4 mm can substantially impact the flow field inside the duct. Hence, there is a considerable rise in the base pressure values, and the magnitude of the base pressure progressively increases with an increase in the rib radius and rib locations from 0.5D to 3D. It is seen that for rib location at 66 mm, the gain in

the base pressure values is maximum as 3D seems to be a reattachment point also, where the flow will interact with the secondary vortices formed at the reattachment point due to the sharp corners of the ribs. Apart from this, the waves formed at the nozzle exit will interact with the duct wall and push some mass toward the recirculation region, increasing the base pressure. There is a marginal reduction in the base pressure for all the rib locations for more considerable duct lengths. The ambient pressure cannot influence the flow inside the duct, which otherwise can impact lower duct lengths. The outcomes of this research are nothing more than the technological demonstration, and one can select a combination of rib radius, rib location, duct length, and level of expansion based on the end-user requirements.

References

[1] Pathan, Khizar Ahmed, Prakash S. Dabeer, and Sher Afghan Khan. "Effect of nozzle pressure ratio and control jet location to control base pressure in suddenly expanded flows." *Journal of Applied Fluid Mechanics* 12, no. 4 (2019): 1127-1135. https://doi.org/10.29252/jafm.12.04.29495

[2] Pathan, Khizar Ahmed, Syed Ashfaq, Prakash S. Dabeer, and Sher Afgan Khan. "Analysis of Parameters Affecting Thrust and Base Pressure in Suddenly Expanded Flow from Nozzle." *Journal of Advanced Research in Fluid Mechanics and Thermal Sciences* 64, no. 1 (2019): 1-18.

[3] Fiqri, Muhammad Ikhwan, Khizar Ahmed Pathan, and Sher Afghan Khan. "Control of Suddenly Expanded Flow with Cavity at Sonic Mach Number." In *International Conference on Advances in Heat Transfer and Fluid Dynamics*, pp. 3-15. Singapore: Springer Nature Singapore, 2022. https://doi.org/10.1007/978-981-99-7213-5_1

[4] Asadullah, Mohammed, Sher Afghan Khan, Waqar Asrar, and E. Sulaeman. "Low-cost base drag reduction technique." *International Journal of Mechanical Engineering and Robotics Research* 7, no. 4 (2018): 428-432. https://doi.org/10.18178/ijmerr.7.4.428-432

[5] Pathan, Khizar A., Prakash S. Dabeer, and Sher A. Khan. "Enlarge duct length optimization for suddenly expanded flows." *Advances in Aircraft and Spacecraft Science* 7, no. 3 (2020): 203-214.

[6] Pathan, Khizar Ahmed, Prakash S. Dabeer, and Sher Afghan Khan. "Influence of expansion level on base pressure and reattachment length." *CFD Letters* 11, no. 5 (2019): 22-36.

[7] Azami, Muhammed Hanafi, Mohammed Faheem, Abdul Aabid, Imran Mokashi, and Sher Afghan Khan. "Inspection of supersonic flows in a CD nozzle using experimental method." *International Journal of Recent Technology and Engineering* 8, no. 2S3 (2019): 996-999. https://doi.org/10.35940/ijrte.B1186.0782S319

[8] Pathan, Khizar Ahmed, Zakir Ilahi Chaudhary, Ajaj Rashid Attar, Sher Afghan Khan, and Ambareen Khan. "Optimization of Nozzle Design for Weight Reduction using Variable Wall Thickness." *Journal of Advanced Research in Fluid Mechanics and Thermal Sciences* 112, no. 2 (2023): 86-101. https://doi.org/10.37934/arfmts.112.2.86101

[9] Azami, Muhammed Hanafi, Mohammed Faheem, Abdul Aabid, Imran Mokashi, and Sher Afghan Khan. "Experimental research of wall pressure distribution and effect of micro jet at Mach 1.5." *International Journal of Recent Technology and Engineering* 8, no. 2S3 (2019): 1000-1003. https://doi.org/10.35940/ijrte.B1187.0782S319

[10] Khan, Sher Afghan, Abdul Aabid, and Ahamed Saleel Chandu Veetil. "Influence of micro-jets on the flow development in the enlarged duct at supersonic Mach number." *International Journal of Mechanical and Mechatronics Engineering* 19, no. 1 (2019): 70-82.

[11] Khan, Sher Afghan, and E. Rathakrishnan. "Active control of suddenly expanded flows from under-expanded nozzles-Part II." *International Journal of Turbo and Jet Engines* 22, no. 3 (2005): 163-184. https://doi.org/10.1515/TJJ.2005.22.3.163

[12] Shaikh, Javed S., Krishna Kumar, Khizar A. Pathan, and Sher A. Khan. "Analytical and computational analysis of pressure at the nose of a 2D wedge in high-speed flow." *Advances in Aircraft and Spacecraft Science* 9, no. 2 (2022): 119-130.

[13] Shamitha, Shamitha, Asha Crasta, Khizer Ahmed Pathan, and Sher Afghan Khan. "Numerical simulation of surface pressure of a wedge at supersonic Mach numbers and application of design of experiments." *Journal of Advanced Research in Applied Mechanics* 101, no. 1 (2023): 1-18. https://doi.org/10.37934/aram.101.1.118

[14] Shamitha, Shamitha, Asha Crasta, Khizar Ahmed Pathan, and Sher Afghan Khan. "Analytical and Numerical Simulation of Surface Pressure of an Oscillating Wedge at Hypersonic Mach Numbers and Application of Taguchi's Method." *Journal of Advanced Research in Applied Sciences and Engineering Technology* 30, no. 1 (2023): 15-30. https://doi.org/10.37934/araset.30.1.1530

[15] Shaikh, Javed Shoukat, Khizar Ahmed Pathan, Krishna Kumar, and Sher Afghan Khan. "Effectiveness of Cone Angle on Surface Pressure Distribution along Slant Length of a Cone at Hypersonic Mach Numbers." *Journal of Advanced*

Research in Fluid Mechanics and Thermal Sciences 104, no. 1 (2023): 185-203. https://doi.org/10.37934/arfmts.104.1.185203

[16] Shaikh, Javed S., Krishna Kumar, Khizar A. Pathan, and Sher A. Khan. "Computational analysis of surface pressure distribution over a 2D wedge in the supersonic and hypersonic flow regimes." *Fluid Dynamics & Materials Processing* 19, no. 6 (2023). https://doi.org/10.32604/fdmp.2023.025113

[17] Khan, Sher Afghan, M. A. Fatepurwala, and K. N. Pathan. "CFD analysis of human-powered submarine to minimize drag." *International Journal of Mechanical and Production Engineering Research and Development (IJMPERD)* 8, no. 3 (2018): 1057-1066. https://doi.org/10.24247/ijmperdjun2018111

[18] Pathan, Khizar A., Sher A. Khan, N. A. Shaikh, Arsalan A. Pathan, and Shahnawaz A. Khan. "An investigation of boattail helmet to reduce drag." *Advances in Aircraft and Spacecraft Science* 8, no. 3 (2021): 239.

[19] Fakhruddin, Ahmad 'Afy Ahmad, Fharukh Ahmed Ghasi Mahaboobali, Ambareen Khan, Mohammad Nishat Akhtar, Sher Afghan Khan, and Khizar Ahmad Pathan. "Analysis of Base Pressure Control with Ribs at Mach 1.2 using CFD Method." *Journal of Advanced Research in Fluid Mechanics and Thermal Sciences* 123, no. 1 (2024): 108-143. https://doi.org/10.37934/arfmts.123.1.108143

[20] Khan, Ambareen, Parvathy Rajendran, Junior Sarjit Singh Sidhu, S. Thanigaiarasu, Vijayanandh Raja, and Qasem Al-Mdallal. "Convolutional neural network modeling and response surface analysis of compressible flow at sonic and supersonic Mach numbers." *Alexandria Engineering Journal* 65 (2023): 997-1029. https://doi.org/10.1016/j.aej.2022.10.006

[21] Khan, Ambareen, Parvathy Rajendran, Junior Sarjit Singh Sidhu, and Mohsen Sharifpur. "Experimental investigation of suddenly expanded flow at sonic and supersonic Mach numbers using semi-circular ribs: a comparative study between experimental, single layer, deep neural network (SLNN and DNN) models." *The European Physical Journal Plus* 138, no. 4 (2023): 314. https://doi.org/10.1140/epjp/s13360-023-03853-1

[22] Chaudhari, Pavan Bhaskar, Rachayya Arakerimath, Khizar Ahmed Pathan, and Sher Afghan Khan. "Comparative Experimental Analysis and Performance Optimization of Single-Cylinder DI and HCCI Engine with Series Catalytic Converters." *Journal of Advanced Research in Fluid Mechanics and Thermal Sciences* 121, no. 1 (2024): 173-187. https://doi.org/10.37934/arfmts.121.1.173187

[23] Jain, Yogeshkumar, Vijay Kurkute, Sagar Mane Deshmukh, Khizar Ahmed Pathan, Ajaj Rashid Attar, and Sher Afghan Khan. "The Influence of Plate Fin Heat Sink Orientation under Natural Convection on Thermal Performance: An Experimental and Numerical Study." *Journal of Advanced Research in Fluid Mechanics and Thermal Sciences* 114, no. 2 (2024): 118-129. https://doi.org/10.37934/arfmts.114.2.118129

[24] Khalil, Shaikh Sohel Mohd, Rai Sujit Nath Sahai, Nitin Parashram Gulhane, Khizar Ahmed Pathan, Ajaj Rashid Attar, and Sher Afghan Khan. "Experimental Investigation of Local Nusselt Profile Dissemination to Augment Heat Transfer under Air Jet Infringements for Industrial Applications." *Journal of Advanced Research in Fluid Mechanics and Thermal Sciences* 112, no. 2 (2023): 161-173. https://doi.org/10.37934/arfmts.112.2.161173

[25] Shaikh, Sohel Khalil, Khizar Ahmed Pathan, Zakir Ilahi Chaudhary, B. G. Marlpalle, and Sher Afghan Khan. "An investigation of three-way catalytic converter for various inlet cone angles using CFD." *CFD Letters* 12, no. 9 (2020): 76-90. https://doi.org/10.37934/cfdl.12.9.7690

[26] Shaikh, Sohel Khalil, Khizar Ahmed Pathan, Zakir Ilahi Chaudhary, and Sher Afghan Khan. "CFD analysis of an automobile catalytic converter to obtain flow uniformity and to minimize pressure drop across the monolith." *CFD Letters* 12, no. 9 (2020): 116-128. https://doi.org/10.37934/cfdl.12.9.116128

[27] Kale, Dipak, Rachayya Arakerimath, Khizar Ahmed Pathan, and Sher Afghan Khan. "Investigation on Water Erosion Behavior of Ti-based Metal Matrix Composite: Experimental Approach." *Journal of Advanced Research in Fluid Mechanics and Thermal Sciences* 122, no. 2 (2024): 71-82. https://doi.org/10.37934/arfmts.122.2.7182

[28] Sheikh, Fahim Rahim, Suresh Pandurang Deshmukh, Purushottam Ardhapurkar, Khizar Ahmed Pathan, Sohel Khalil Shaikh, and Sher Afghan Khan. "Modeling and Experimental Validation of NePCM-Nanofluid-Based PVT System." *Journal of Advanced Research in Fluid Mechanics and Thermal Sciences* 122, no. 1 (2024): 205-222. https://doi.org/10.37934/arfmts.122.1.205222

[29] Khan, Ambareen, Abdul Aabid, Sher Afghan Khan, Mohammad Nishat Akhtar, and Muneer Baig. "Comprehensive CFD analysis of base pressure control using quarter ribs in sudden expansion duct at sonic Mach numbers." *International Journal of Thermofluids* 24 (2024): 100908. https://doi.org/10.1016/j.ijft.2024.100908

[30] Khan, Ambareen, Sher Afghan Khan, Vijayanandh Raja, Abdul Aabid, and Muneer Baig. "Effect of ribs in a suddenly expanded flow at sonic Mach number." *Heliyon* 10, no. 9 (2024). https://doi.org/10.1016/j.heliyon.2024.e30313

[31] Khan, Ambareen, Sher Afghan Khan, Mohammed Nishat Akhtar, Abdul Aabid, and Muneer Baig. "Base Pressure Control with Semi-Circular Ribs at Critical Mach Number." *Fluid Dynamics & Materials Processing* 20, no. 9 (2024). https://doi.org/10.32604/fdmp.2024.049368

[32] Nurhanis, Tun, Ambareen Khan, Mohammad Nishat Akhtar, and Sher Afghan Khan. "Control of Base Pressure at Supersonic Mach Number in a Suddenly Expanded Flow." *Journal of Advanced Research in Fluid Mechanics and Thermal Sciences* 109, no. 1 (2023): 210-225. https://doi.org/10.37934/arfmts.109.1.210225
[33] Khan, Ambareen, Nurul Musfirah Mazlan, and Mohd Azmi Ismail. "Velocity Distribution and Base Pressure Analysis of Under Expanded Nozzle Flow at Mach 1.0." *Journal of Advanced Research in Fluid Mechanics and Thermal Sciences* 92, no. 1 (2022): 177-189. https://doi.org/10.37934/arfmts.92.1.177189
[34] Khan, Ambareen, Nurul Musfirah Mazlan, and Ervin Sulaeman. "Effect of Ribs as Passive Control on Base Pressure at Sonic Mach Numbers." *CFD Letters* 14, no. 1 (2022): 140-151. https://doi.org/10.37934/cfdl.14.1.140151
[35] Khan, Ambareen, Mohd Azmi Ismail, and Nurul Musfirah Mazlan. "Numerical Simulation of Suddenly Expanded Flow from Converging Nozzle at Sonic Mach Number." In *Proceedings of International Conference of Aerospace and Mechanical Engineering 2019: AeroMech 2019*, 20-21 November 2019, Universiti Sains Malaysia, Malaysia, pp. 349-359. Springer Singapore, 2020. https://doi.org/10.1007/978-981-15-4756-0_29
[36] Khan, Ambareen, Nurul Musfirah Mazlan, and Mohd Azmi Ismail. "Analysis of flow through a convergent nozzle at Sonic Mach Number for Area Ratio 4." *Journal of Advanced Research in Fluid Mechanics and Thermal Sciences* 62, no. 1 (2019): 66-79.
[37] Khan, Ambareen, Nurul Musfirah Mazlan, Mohd Azmi Ismail, and Mohammad Nishat Akhtar. "Experimental and numerical simulations at sonic and supersonic Mach numbers for area ratio 7.84." *CFD Letters* 11, no. 5 (2019): 50-60.
[38] Rathakrishnan, E. "Effect of ribs on suddenly expanded flows." *AIAA Journal* 39, no. 7 (2001): 1402-1404. https://doi.org/10.2514/2.1461